Dürig, T., Gudmundsson, M. T., Dioguardi, F., Woodhouse, M., Björnsson, H., Barsotti, S., Witt, T., Walter, T. R. (2018): REFIR- A multi-parameter system for near real-time estimates of plume-height and mass eruption rate during explosive eruptions. - *Journal of Volcanology and Geothermal Research*, *360*, pp. 61—83.

DOI: http://doi.org/10.1016/j.jvolgeores.2018.07.003

Journal of Volcanology and Geothermal Research 360 (2018) 61–83

Contents lists available at ScienceDirect

Journal of Volcanology and Geothermal Research

journal homepage: www.elsevier.com/locate/jvolgeores

REFIR- A multi-parameter system for near real-time estimates of plume-height and mass eruption rate during explosive eruptions

Tobias Dürig [a,b,*], Magnús T. Gudmundsson [a], Fabio Dioguardi [c], Mark Woodhouse [d], Halldór Björnsson [e], Sara Barsotti [e], Tanja Witt [f], Thomas R. Walter [f]

[a] Institute of Earth Sciences, University of Iceland, Sturlugata 7, 101 Reykjavík, Iceland
[b] Geology Department, University of Otago, 360 Leith Street, Dunedin 9016, New Zealand
[c] British Geological Survey, The Lyell Centre, Research Avenue South, Edinburgh EH14 4AP, UK
[d] School of Earth Science, University of Bristol, Wills Memorial Building, Queen's Road, Bristol BS8 1RJ, UK
[e] Icelandic Meteorological Office, Bústaðavegi 7- 9, 108 Reykjavík, Iceland
[f] GFZ-German Research Center for Geosciences, Helmholtzstraße 6/7, 14467 Potsdam, Germany

ARTICLE INFO

Article history:
Received 30 March 2018
Received in revised form 7 July 2018
Accepted 7 July 2018
Available online 18 July 2018

Keywords:
Real-time eruption monitoring
Operational use
Plume heights
Mass eruption rate
Volcanic plume models

ABSTRACT

Meaningful forecasting of the atmospheric concentration and ground accumulation of volcanic ash during explosive eruptions requires detailed knowledge of the eruption source parameters. However, due to the large uncertainties in observations and limitations of current models used to make inferences from these, monitoring an ongoing eruption and quantifying the mass eruption rate in real-time is a considerable challenge. Within the EU supersite project "FutureVolc", an integrated approach has been applied to develop a quasi-autonomous multi-parameter system, denoted "REFIR", for monitoring volcanic eruptions in Iceland and assessing the eruption mass flow rate by inverting the plume height information and taking account of these uncertainties. REFIR has the capability to ingest and process streaming plume-height data provided by a multitude of ground based sensors, including C– and X-band radars and web-cam based plume height tracking systems. These observational data are used with a suite of plume models that also consider the current wind and other atmospheric conditions, providing statistically assessed best estimates of plume height and mass eruption rate. Provided instrumental data is available, near real-time estimates are obtained (the delay corresponding to the scan rate of data-providing instruments, presently of the order of minutes). Using the Hekla 2000, and Eyjafjallajökull 2010 eruptions in Iceland, the potential of REFIR is demonstrated and discussed through application to three scenarios. The system has been developed to provide maximum flexibility. A setup script assists the user in adapting to local conditions, allowing implementation of REFIR for any volcanic eruption site worldwide. REFIR is designed to be easily upgradable, allowing future extension of monitoring networks, learning from new events, and incorporation of new technologies and model improvements. This article gives an overview of the basic structure, models implemented, functionalities and the computational techniques of REFIR.

1. Introduction

Tephra injected into the atmosphere during explosive volcanic eruptions poses a direct threat to aviation and when it falls to the ground it can have widespread primary and secondary impacts at different spatial and temporal scales (Simkin et al. 2001, Jenkins et al. 2015). Volcanic particles can cause damage to aircraft turbines and engines (Durant et al., 2010; Chen and Zhao, 2015; Giehl et al., 2017), and mitigation through airspace management during explosive eruptions causes travel disruptions that can potentially affect large areas (see, e.g., Guffanti et al., 2010; Guffanti and Tupper, 2015). The accumulation of tephra can damage buildings (e.g., Blong 1981, Spence et al., 2005), critical infrastructure, water reservoirs, crops (Wilson et al., 2012 and 2014) and can significantly reduce renewable energy production even at large distances from the source (Zorn and Walter, 2016). Fine volcanic ash (grain sizes < 63 μm) may cause short-term health problems in susceptible individuals or longer-term health problems if individuals are exposed to ash repeatedly for long periods of time (Baxter et al., 1999; Horwell and Baxter, 2006; Damby et al., 2017). The 2010 eruption of Eyjafjallajökull (Iceland) represents an example of how a relatively modest eruption, if long lasting, can impact air traffic over continental scales and for long periods (Harris et al., 2012). Following the disruption caused by this eruption, the volcanological community invested a significant effort into the improvement of observational and modelling

* Corresponding author at: Geology Department, University of Otago, 360 Leith Street, Dunedin 9016, New Zealand
E-mail address: tobias.durig@otago.ac.nz (T. Dürig).

https://doi.org/10.1016/j.jvolgeores.2018.07.003

techniques for tracking ash clouds in the atmosphere and forecasting their spatio-temporal evolution. In particular, forecasting the concentration of ash in the atmosphere requires detailed knowledge of both parameters that describe eruptive conditions, referred to here as the eruption source parameters (Woods, 1988; Sparks 1997; Mastin et al., 2009, Dellino et al., 2014), and those describing atmospheric conditions (Hewett et al., 1971; Bursik, 2001; Degruyter and Bonadonna, 2012, 2013; Devenish, 2013; Woodhouse et al., 2013, 2015; Costa et al., 2016; Macedonio et al., 2016). Of particular importance is the rate at which material is ejected by the volcano, known as the mass flux or, "mass eruption rate" (Wilson and Walker, 1987). Mass eruption rate (MER) represents a crucial input parameter of models that are currently used for simulating dispersion of volcanic ash in the atmosphere (e.g. Mastin et al., 2013; Bonadonna et al., 2012; Folch, 2012; Folch et al. 2009; Barsotti et al., 2008; Jones et al., 2007; Costa et al., 2006). MER cannot currently be measured directly at the volcanic vent but several efforts are being made towards the development of approaches that integrate different monitoring techniques such as time-lapse and high-speed pixel tracking (Walter, 2011; Taddeucci et al., 2015), measuring emitted infra-sound waves (Johnson and Ripepe, 2011; Ripepe et al., 2013), thermal infrared signatures (Valade et al., 2014, Cerminara et al., 2015) or changes in the electrostatic field (Büttner et al., 2000; Calvari et al., 2012). The accuracy of MER estimates may, for example, be improved by linking satellite-based automatic ash plume analysis methods (e.g. Gouhier et al., 2012, 2015; Pouget et al., 2016) with ground-based video analysis (e.g., Scollo et al., 2014; Witt and Walter, 2017) or Doppler-radar plume tracking methods (see e.g., Donnadieu et al., 2016). Until now, an indirect approach has typically been employed that links the observed properties of the volcanic cloud (in particular plume height) to the source parameters and the atmospheric conditions. The characteristics and the dynamics of the eruptive column are closely linked to the source (Sparks, 1997; Carazzo et al., 2008; Mastin et al., 2009; Dellino et al., 2014; Dürig et al., 2015a, 2015b; Dioguardi et al., 2016) and the wind conditions (Bursik, 2001; Degruyter and Bonadonna, 2012, 2013; Devenish, 2013; Woodhouse et al., 2013; Mastin, 2014).

The relationship between source conditions and plume height (with or without the effect of wind) has been described using mathematical models of turbulent eruption columns (e.g., Morton et al., 1956). Numerous strategies for the calculation of MER are available in the volcanological literature. Elaborate 3D models have been developed (e.g., Oberhuber et al., 1998; Esposti Ongaro et al., 2007; Suzuki et al., 2016; Cerminara et al., 2016a) and are able to capture the details of plume dynamics (Cerminara et al., 2016b) but, due to their high computational demand, are currently not suitable for plume simulations in real-time given the available computational resources. Real-time assessment hence requires the application of simple empirical or theoretical laws often referred to as "0D" models or "1D" models solving for the conservation of mass, momentum and energy along the time-averaged trajectory.

0D models can be either empirical or theoretical. Empirical models result from the regression analyses between plume height and MER of past eruptions (e.g. Sparks, 1997; Mastin et al., 2009; Aubry et al. 2017) that can be further calibrated for specific cases (e.g. Gudmundsson et al., 2012). Theoretical models emerge from an analysis of fluid dynamics of turbulent jets and plumes that leads to the

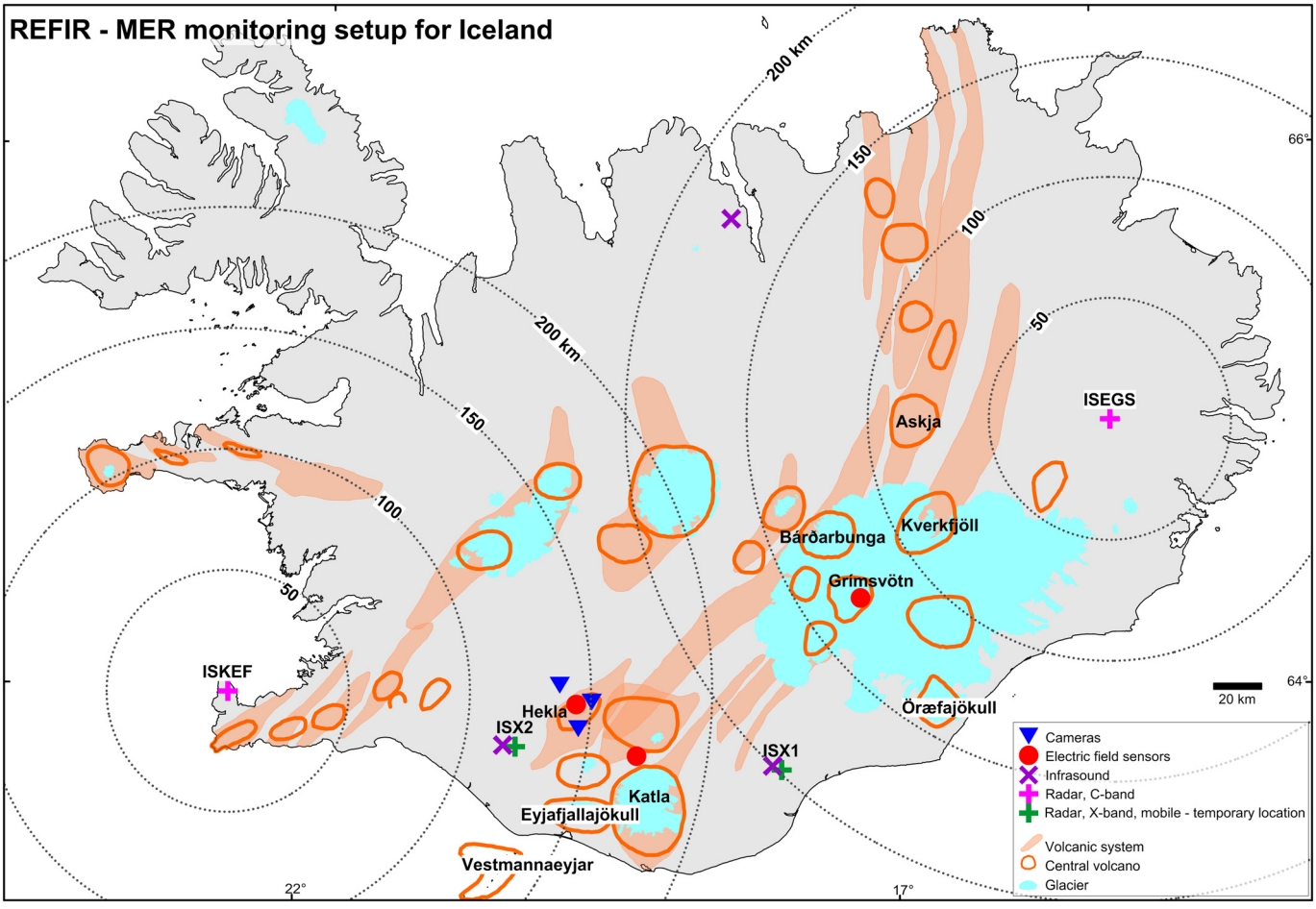

Fig. 1. Positions of volcanoes and sensors in Iceland used by REFIR when installing the system in its default ("FutureVolc") configuration. When changes are made to the sensor setup or once the eruption site location is precisely known, coordinates can be changed by updating the corresponding ".ini" files.

relationship between the maximum plume height and the mass flux at the source (Morton et al., 1956). These have been later modified to take into account the effect of a crossflow (e.g. wind) (Hewett et al. 1971) and applied to the volcanic case (e.g. Degruyter and Bonadonna, 2012; Woodhouse et al. 2013).

1D integral models are based on a mathematical description of turbulent buoyant plumes in which transient turbulent processes are 'averaged' so that turbulent mixing is modelled through an entrainment parameterization, following Morton et al. (1956). In order to obtain MER from the observed plume height with 1D models, a model inversion is required and an iterative procedure is employed. A starting value for MER is assumed, the governing equations are solved and a prediction for the plume height h^* obtained and compared with an observation, leading to a refinement of the boundary conditions until an acceptable match between the height observation and the model prediction is achieved. In this paper, we refer to Costa et al. (2016) for a detail review of the available 1D models, since REFIR computations are based on the 0D models. A 1D model (Woodhouse et al. 2013) can be optionally invoked as an external routine (see Section 3.2.1.1).

In an ideal scenario, MER is provided in (quasi) real time to volcanic cloud dispersion modellers in order to obtain a continuously updated prediction of how and to what extent volcanic products are transported in the atmosphere. However, monitoring an ongoing eruption for the time-changing plume height is a considerable challenge and is affected by uncertainties that propagate into the MER estimation and dispersion models. The MER estimates include uncertainties implicit in the model used to derive them, such as epistemic uncertainties in model parameters, aleatory uncertainty in model forcings (e.g. atmospheric conditions) and structural uncertainties in the model formulation (e.g. approximate descriptions of turbulent mixing) (Woodhouse et al., 2015).

Following the strategy of integrating a wide-ranging set of sensors capable of providing observational information on the eruption source, and combining several approaches to calculate MER, rather than relying on one single method, a quasi-autonomous real-time multi-parameter system, called REFIR (**R**eal-time **E**ruption source parameters **F**utureVolc **I**nformation and **R**econnaissance system, see supplement S1), has been developed within FutureVolc, a project funded by the FP7 Environment Programme of the European Commission (futurvolc.hi.is; final report can be accessed on: http://cordis.europa.eu/result/rcn/189791_en.html). The system was designed to make use of manually entered information as well as streaming data by a multitude of sensors, including C-band radars (i.e., radar operating on frequencies ranging from 4 to 8 GHz), X-band radars (operating on frequencies of 8–12 GHz), webcam based plume height tracking systems, imaging ultra-violet and infrared cameras and electric field sensors. The plume-height data coming from those different sources are processed by the system, which evaluates the specific uncertainties and applies statistical techniques in order to assess and plot the current plume height and its estimated uncertainty range. This important eruption source parameter is used to calculate the MER in near real-time (within a time interval of 5 min) as soon as an eruption has started, based on selected plume models. Different plume models adopt different assumptions and parameterizations and therefore produce differing values of MER. This is taken into account in REFIR as the system computes the "best estimate" of MER by using a statistical approach in combination with user-defined weight factors. During an eruption outputs from REFIR can optionally be made available online.

The system has been developed in such a way that it can be used operationally for a large range of conditions and data availability. The priority has been maximum flexibility, so REFIR requires minimum

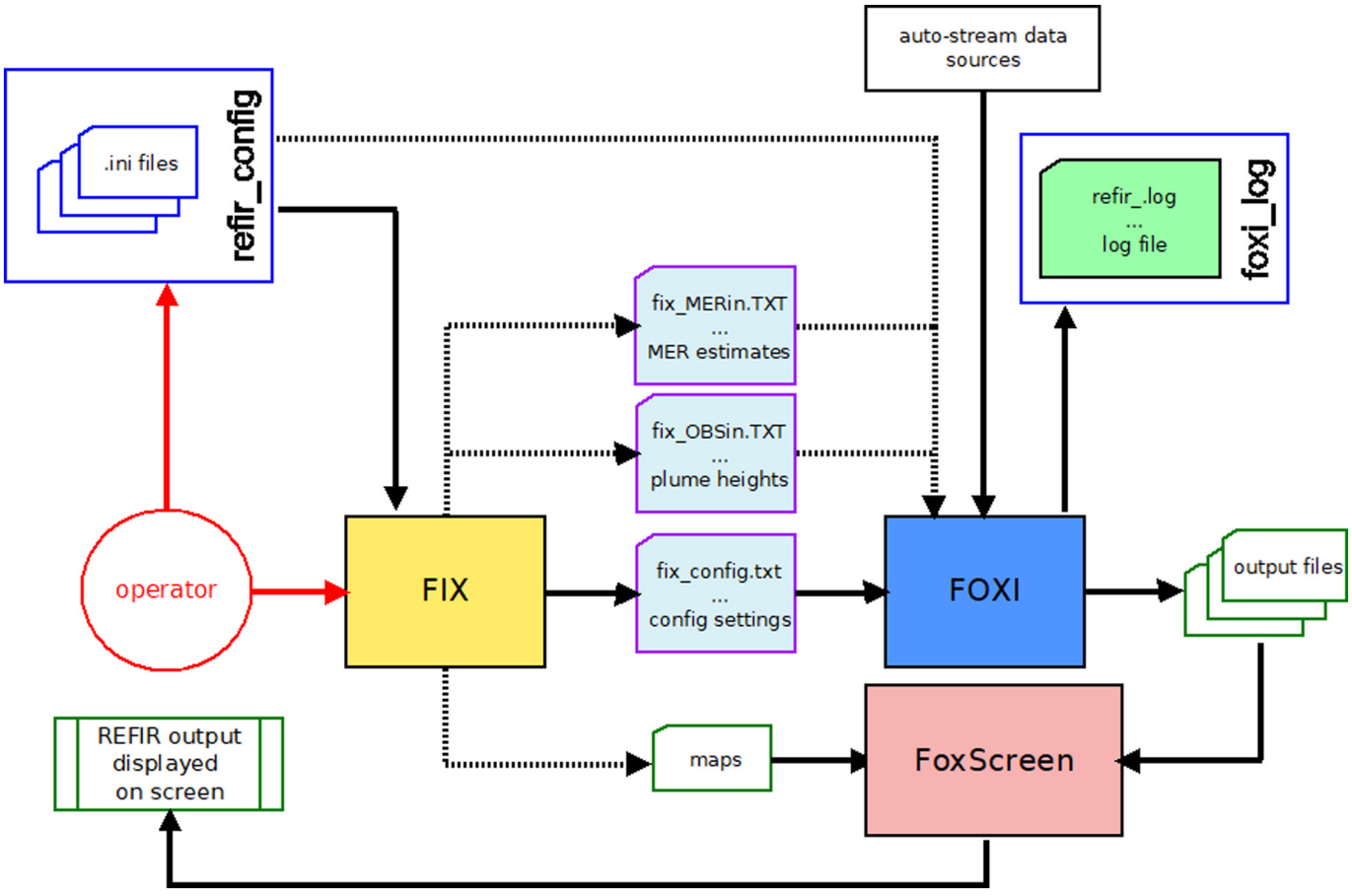

Fig. 2. REFIR components and their intercommunication structure. The key programs of REFIR are the two python scripts FIX.py and FOXI.py, which use mainly the ASCII file fix_config.txt as communication hub.

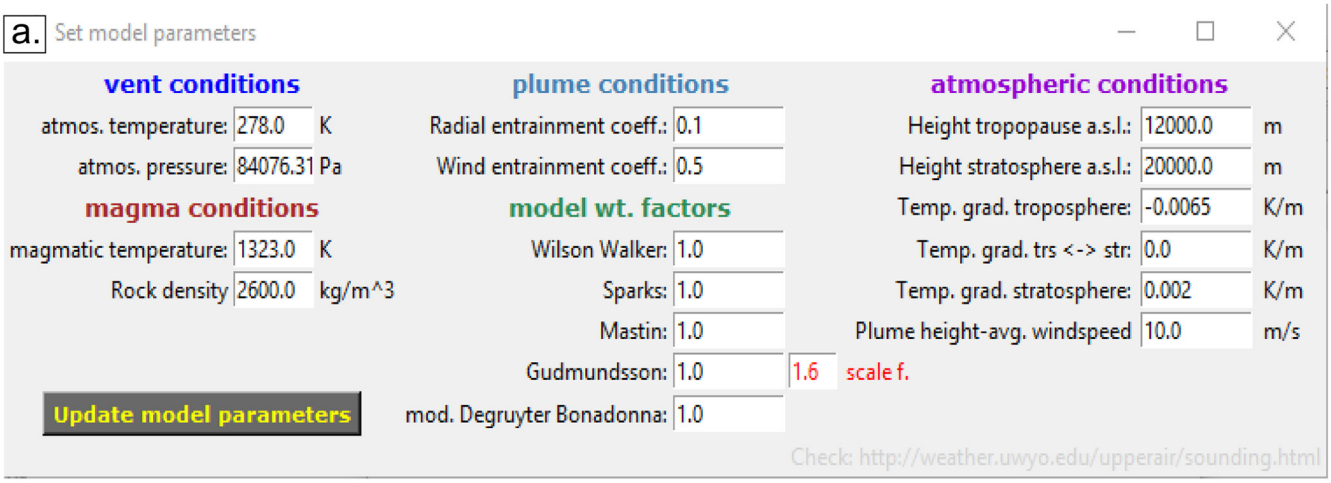

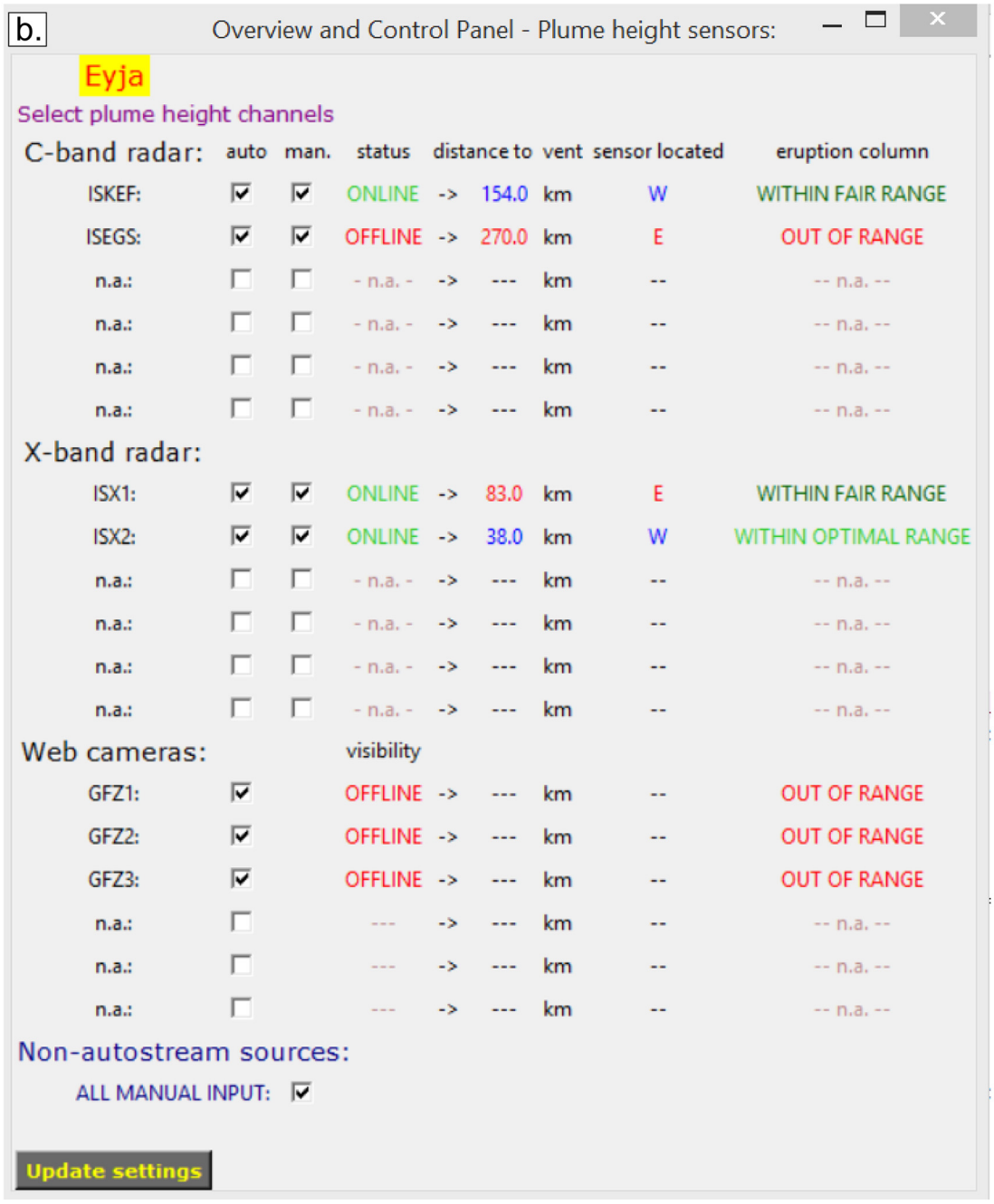

Fig. 3. Screenshots from the GUI provided by FIX.py. This user interface allows the operator, inter alia, to (a) specify the system settings and to (b) control the status of plume height data sources.

adaptation to local conditions (types of volcanoes, monitoring systems, etc.) and can be implemented at any volcano observatory worldwide. Moreover, the system is designed to be easily upgraded by, for example, incorporating new additions in monitoring networks and further refinements in the computational process.

This paper describes the structure, functionalities, the models implemented and the computational techniques of REFIR. More detailed information on the software can be found in the companion manual (see supplement S2). The potential of REFIR is demonstrated and discussed for two test cases, based on monitoring data from two eruptions in Iceland: Hekla in 2000 (Lacasse et al., 2004; Höskuldsson et al., 2007) and Eyjafjallajökull in 2010 (Gudmundsson et al., 2012; Dellino et al., 2012).

2. Description of REFIR

2.1. Target areas and plume height sensors

The REFIR system is currently designed to monitor up to ten volcanoes, whose parameters (name, GPS coordinates and height of the vent) are specified in an initial configuration file ("volcano_list.ini").

In its original Iceland-based "FutureVolc setup", the file includes the volcanoes Eyjafjallajökull, Katla, Hekla, Grímsvötn, Vestmannaeyjar, Bárðarbunga, Kverkfjöll, Öræfajökull and Askja (Fig. 1), which together account for the vast majority of explosive eruptions in Iceland. A tenth slot is reserved to provide capability for an eruption at a previously unspecified location, reflecting the fact that eruptions at unexpected sites are not unknown in Iceland. A real name and coordinates of an actual eruption, if one occurs outside the pre-specified volcanoes, can easily be accommodated by modifying the configuration file using a simple text editor.

REFIR is currently designed to process automatic plume height data streams from up to 3×6 ground-based sensors, which are divided into three classes, based on commonly used plume monitoring instruments in Iceland:

1. "C-band radar sensors": REFIR provides slots for up to six radar sensors of this class.
2. "X-band radar sensors": REFIR provides slots for up to six sensors of this class.
3. "Web cameras": these sensors provide data on both plume height and on current local visibility and the attributed uncertainty. Furthermore, these sensor types are typically focused on a specific volcano. REFIR provides slots for up to six sensors of this class.

The naming of these classes is generic and refer to the setup in Iceland. Thus, "C-band radar" refers to horizontally scanning instruments at a fixed location and not targeted to a specific volcano (indeed volcano plume monitoring may not be the primary role of the instrument, e.g. when using a weather radar station). The "X-band radar" class refers to vertically scanning, mobile instruments brought to a volcano during an eruption, and the "Web cameras" class refers to fixed instruments proximal to volcanoes and dedicated to volcano monitoring.

The name of the classes does not preclude the use of other types of sensors within REFIR. Any kind of sensor capable of automatically providing plume height data streams (e.g. infrared cameras, DOAS or LiDAR) can be incorporated, by assigning them to the one of the three classes to which it fits best. The only requirements for plume height sensors to be used for REFIR are that they should be located at a safe distance from the eruption site to ensure a continuous flow of data, and should be robust enough to withstand potential adverse environmental conditions, for example when exposed to volcanic gases.

For the "FutureVolc setup" in Iceland, seven sensors were included: two C-band radar stations (at Keflavík airport – ISKEF, and Egilsstaðir - ISEGS) operated by the Icelandic Meteorological Office (IMO) and two mobile X-band radars, denoted ISX1 and ISX2, also operated by the IMO. The mobility of the latter sensors ensures that they can record ash columns of all sizes (i.e., in theory ranging from Strombolian to ultra-Plinian) at any eruption site in Iceland. Furthermore, three automatic plume-tracking cameras from Mobotix (one modified D14D and two M14 web-cams) have been mounted, denoted CAM1, CAM2 and CAM3. The cameras are calibrated and used as threefold auto-tracker: first to estimate weather conditions during eruption, second to calculate plume heights using a Sobel edge detection techniques approach (see, e.g., Witt and Walter, 2017) and third to track pixels using particle image velocimetry.

In addition, REFIR ingests plume height data manually added by the user, offering the option to either specify the source of the entered information (in which case REFIR will automatically assign the source-specific uncertainties to the data set) or to quantify the range of plume heights directly.

2.2. The REFIR components and their communication structure

REFIR is a package of python scripts and text files that store, organize, process, communicate and report data obtained through input streams (see Fig. 2). For details on the individual files, the reader is referred to the companion manual (see supplement S2). In this paper we focus on three main components:

1. FIX.py provides a graphical user interface (GUI) that displays the status of data sources (e.g. radar stations) and allows the system operator to control all input and boundary parameters needed for the computation of the current MER (see Fig. 3). The script retrieves the relevant parameters of the selected volcano from the initialization files and generates or updates the configuration file "fix_config.txt". In addition, FIX.py provides also an interface to manually add plume height, plume width and MER information.
2. FOXI.py, a python program which reads the data streams and computes MER by constantly iterating a sequence of processes with a repetition rate of 5 min.
3. FoxScreen.py arranges output files generated by FIX.py and FOXI.py in an overview window. Since it serves solely the purpose of data presentation, FoxScreen.py is not required for running REFIR.

While the programs FIX.py and FoxScreen.py are the main interfaces between the operator and the system, the actual data processing is conducted within the program FOXI.py. The communication link between FIX.py and FOXI.py is provided by the configuration data file ("fix_config.txt"). Information on plume heights, plume width and MER can be manually entered using FIX.py and is saved and transferred to FOXI.py via additional text files (denoted "fix_OBSin.txt" and "fix_MERin.txt", respectively). FIX.py and FOXI.py are the key programs of REFIR, with FOXI.py being its core element.

2.3. Plume height data streams: Uncertainties and quality factors

REFIR distinguishes between two main categories of plume height information:

- "auto-stream data": data which is streamed automatically
- "manual entry data": data which is manually entered by the system operator, using the FIX.py user interface

The latter option can be chosen if, for example, the plume height data from pilot reports or ground observation should be included, or if the uplink to a correctly working radar station is defective, but plume height information is received by telephone transmission.

Fig. 4 illustrates the "FutureVolc setup" of REFIR which features up to 12 data channels (7 auto-stream and 5 manual entry). In general, the system in its current version can be operated with plume height data

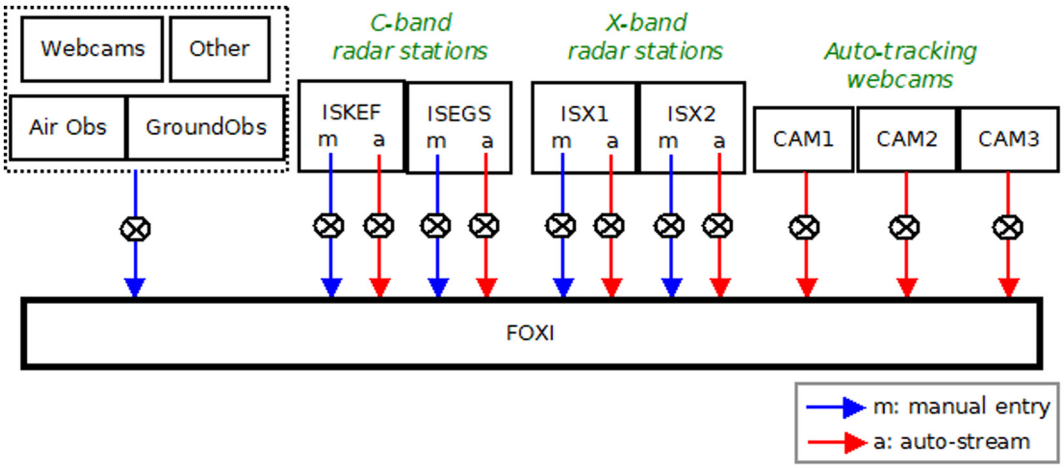

Fig. 4. Plume height data channels that can be controlled by the operator (with crossed circles illustrating switches). Auto-stream channels ("a") are marked by red arrows, while manual entries ("m") are fed via channels marked in blue. This example refers to the Icelandic FutureVolc setting.

imported via up to 31 channels (i.e., 18 auto-stream channels and 13 manual entry channels), which can be individually controlled by the system operator (see Fig. 3b). This allows the operator to have maximum control over all plume height input data and avoid problems that occur when encountering misleading data from a malfunctioning sensor by simply switching off the corresponding data channel.

For each datum received, the system automatically assigns the corresponding error margin, depending on the plume height sensor used (see Table 1).

For the auto-tracking web cams REFIR uses default uncertainties automatically provided by this class of sensors based on automated analysis of the streaming webcam images. The error bars can therefore vary during data streaming, depending, e.g. on the visibility conditions. Along with the plume height value and the uncertainty, the visibility condition is expected to be automatically provided by the webcams as well. For the Iceland setup, for this purpose an in-house developed software is used, which applies photogrammetric methods, matching the frames with known characteristic of the landscape (see manual in supplement S2 for details). The visibility is characterized by a value which ranges from 0 (no visibility) to 4 (optimal visibility). All plume height information of automatic webcams is imported as auto-stream data.

The uncertainties for data from radar sensors is computed following Arason et al. (2011) and considering both the distance between vent and sensor, denoted by d, and the sensor-specific radar beam width, described by the angle δ, the uncertainties of plume height data, denoted by Δh, measured by radar sensors are computed by

$$\Delta h = \frac{1}{2} d \tan\delta. \quad (1)$$

We note that this assignment of the observational uncertainty in the radar data assumes that beam spreading is the dominant component of the measurement error. Radar-derived plume height data can also be entered manually, in which case the interface provides the operator with the option to specify the estimated range of plume heights also by hand.

If added plume height information obtained by air or ground observation is not given with an uncertainty, default values are assigned (see Table 1) based on experiences made in past eruptions (Oddsson et al. 2012, Gudmundsson et al., 2015). The same applies also to data from other sources, for example when entering information derived by the evaluation of satellite images.

Along with the error margins, REFIR also quantifies the expected quality attributed to data from each of the sensors by assigning a quality factor, denoted by q_f, following a decision routine illustrated in Table 2. For radar sensors, q_f ranges from 0 to 3, solely depending on d. In case of auto-tracking webcams, however, the quality factors can range between 0 and 4 and depend exclusively on the visibility condition at the time of the plume height measurement. The quality factors play an important role for finding a best estimate for the current plume height: higher values of q_f correspond to a larger influence of the corresponding datum on the MER estimate.

2.4. The key data processing levels within REFIR

Fig. 5 illustrates the analysis strategy applied by REFIR. Once started, the depicted sequence is iterated every 5 min, which means that the conclusive estimate of MER ("final best estimate", denoted "FMER") is constantly updated in near-real time. Data are processed in a sequence of three main data processing levels (marked by different colors in Fig. 5).

1. At the first level (green in Fig. 5), a best estimate for the current height of the plume top is computed on the basis of the readings provided by the plume height sensors, along with additional observational information that may be available from aircraft and ground teams (Section 3.1).

Table 1
Error margins and quality factors assigned to plume height data. For each datum, REFIR assigns an uncertainty, depending on data source, stream type and option the operator choses.

Source	Stream type	Plume height uncertainty assigned to datum		Range of quality factor q_f
		Default	Optional	
Auto-tracking webcam	Auto	Automatically provided by webcam	–	0–4
Radar sensor (C– or X-band)	Auto	Computed by REFIR, using Eq. (1)	–	0–3
	Manual	Computed by REFIR, using Eq. (1)	Entered by operator	0–3
Air observation	Manual	1000 m	Entered by operator	0–3
Ground observation	Manual	1500 m	Entered by operator	0–3
Other	Manual	1500 m	Entered by operator	0–3

Table 2
Quality factors for data sensor. For radars the factor is dependent on the distance from the vent while for auto-tracking webcams they are dictated by visibility conditions. Note that this classification is specific for the Icelandic "FutureVolc" setting, but can easily be adjusted within the source code.

Radar type	Distance (km)	Displayed text	Quality factor
C-band	<120	Within optimal range	3
	<200	Within fair range	2
	<255	Within limited range	1
	>255	Out of range	0
X-band	<60	Within optimal range	3
	<120	Within fair range	2
	<180	Within limited range	1
	>180	Out of range	0
Auto-tracking webcams		Clear view	4
		Fair visibility	3
		Restricted visibility	2
		Very low visibility	1
		Out of range	0
		Offline	

2. At the second level (marked in blue), a user-specified suite of up to five REFIR-internal plume height models is used to compute predictions of the MER (see Section 3.2.1). Fig. 3a shows the default case, where all five models are activated and equally weighed. The model calculations define a range of possible mass eruption rates, which is further constrained by a routine that provides a first estimate of the currently expected MER, denoted "RMER" (i.e. REFIR-internal MER estimate). These values are further constrained by considering MER estimates made by the wind-affected plume model "PlumeRise" (Woodhouse et al., 2013), which operates external from REFIR, resulting in an interim estimate, named "CMER".
3. At the third level (marked in red), independent MER predictions from experimental systems which will potentially play a major role in future monitoring of volcanic plumes are considered and used to further constrain the mass eruption rate (see Sections 3.2.2–3.2.3), finally leading to the conclusive "best estimate" of the current MER, denoted "FMER" (see Section 3.2.4). Furthermore, an estimate of

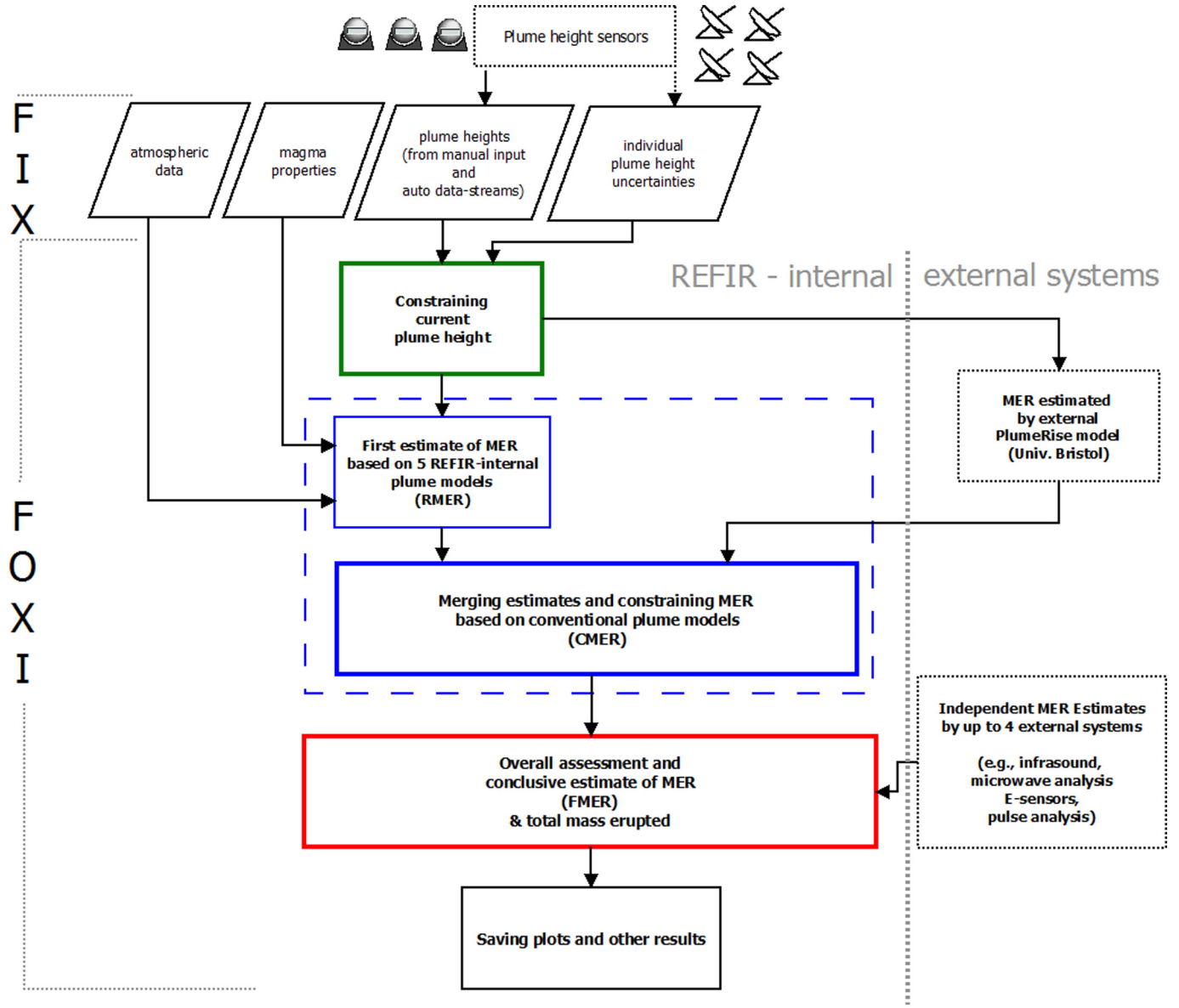

Fig. 5. Schematic illustrating the data flow within REFIR. The three key data processing levels are marked in green, blue and red, respectively. First a best estimate for the plume height is obtained (level 1), then an interim prediction for the MER is computed by using a suite of internal models in combination with an external wind-affected model (level 2). Then external experimental systems are used to further refine the mass eruption rate, resulting in a conclusive best estimate, denoted "FMER", which is also used to calculate the total mass erupted (level 3).

the total erupted mass is obtained by integrating the resulting MER values over time (see Section 3.3).

Details of the key routines applied are described in the following section.

3. Operations performed in FOXI: the calculation of MER

In this section, the method for assessing the best estimate and the range of uncertainty of the plume height as measured by different monitoring techniques is explained. The simplified models implemented in REFIR linking MER to the plume height are then listed and briefly discussed. Finally, the evaluation of the total erupted mass is introduced.

3.1. Plume height assessment

FOXI.py collects plume height data from different automated and manually obtained sources. The time stamps of each data set are noted, and the plume height entries sorted into five time bases:

- 15 minute base: contains only plume height data not older than 15 min
- 30 minute base: contains only plume height data not older than 30 min
- 60 minute base: contains only plume height data not older than 60 min
- 180 minute base: contains only plume height data not older than 3 h
- Auto 30: in this case FOXI.py decides automatically the best time base among 15 or 30 min based on the data that are streaming.

Via FIX.py the system operator can set the time base to be used by FOXI. For example, a radar-based plume height obtained 20 min ago is available within the 30, 60 and 180 min stacks but not within the 15 min stack. Thus, the number of data sets available for further processing depends on (1) the activated data streams and (2) the time base selected by the user (see also Section 5.2).

Based on the collected plume heights within the selected time base and on the number of available data sets (N), FOXI.py carries out a statistical analysis with a reiteration rate of 5 min to obtain the best estimate of the plume height (h). This value is then used to calculate the mass eruption rate. There are four possible scenarios given a selected time base (Fig. 6):

1) The analyzed time base is empty ($N = 0$): no data available, it is not possible to constrain a value of plume height. In this case FOXI.py skips all further steps and jumps to the end of the loop. No MER estimate is generated in this run, and the script is paused for 5 min, waiting for new data.
2) Only one data set (e.g. readings from one radar station) is available ($N = 1$): the best estimate is set as the average value of the constrained plume heights for the single data set.

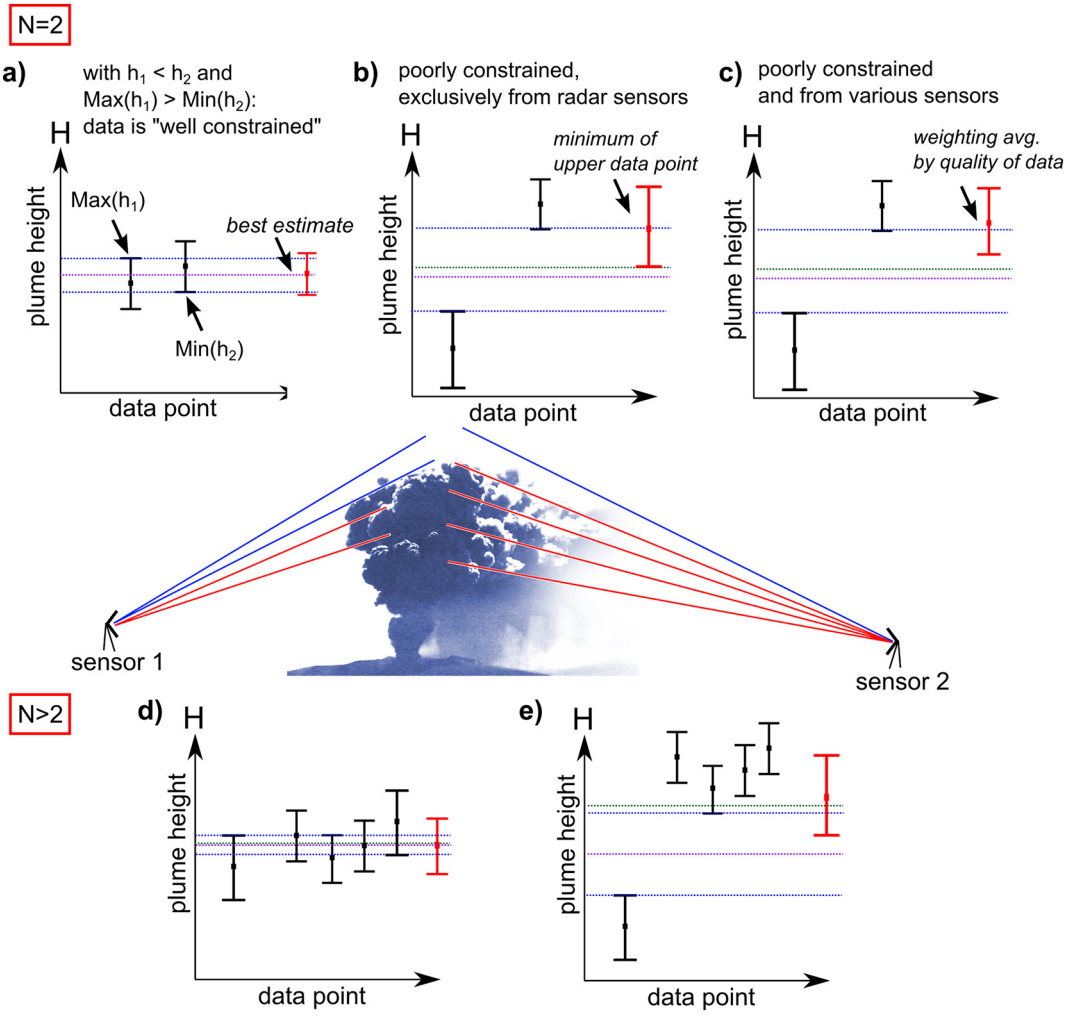

Fig. 6. Procedures followed by REFIR to constrain plume heights in order to find a best estimate.

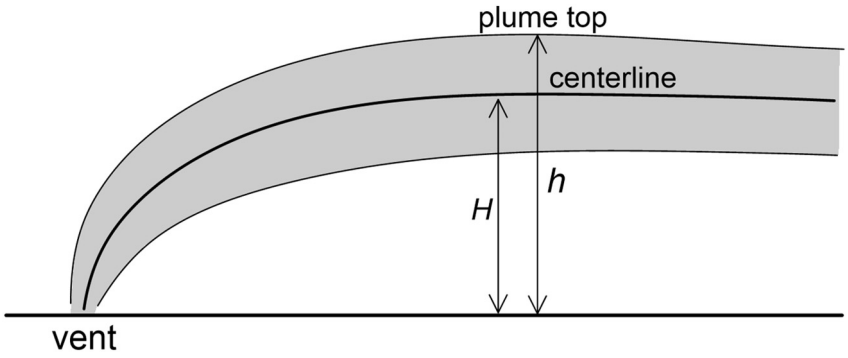

Fig. 7. Schematic illustration of top plume height *h* and center-line plume height *H*.

3) Two data sets (e.g. readings from two radar stations or from one radar station and webcams) are available ($N = 2$): FOXI.py distinguishes between three different scenarios:

- if the maximum value of the data set with the lower plume height lies above the minimum value of the data set with the higher plume height, then FOXI.py considers the data to be *well constrained* and the average of the two data sets is taken as the best estimate (see Fig. 6a). The range of variation is denoted by *s* and is defined as

$$s = \sqrt{\frac{\Delta h_1{}^2 + \Delta h_2{}^2}{2}}, \tag{2}$$

Table 3
Formulas used to compute the interim and final results for MER. MER_i stands for the MER prediction using the following model: $i = 1$: Wilson Walker, $i = 2$: Sparks, $i = 3$: Mastin, $i = 4$: Gudmundsson, $i = 5$: modified Degruyter Bonadonna, $i = 6$: PlumeRise. For a detailed description, see also the companion manual (supplement S2). w_i: model-specific weight factors; f_i: weight factors specific for experimental sensor. $MER_{exp\min,i}$, $MER_{expavg,i}$, $MER_{exp\max,i}$: minimum, average and maximum MER prediction of experimental sensor *i*. a_i: weight factor for *i*-th manually added MER value. $MER_{man\min,i}$, $MER_{manavg,i}$, $MER_{man\max,i}$: *i*-th manually added minimum, average and maximum MER value. N_{man}: number of manually added data sets. The weight for the conventional model output in relation to that for experimental sensors and manually added information is given by the operator-defined factors a_{conv}, a_{exp} and a_{man}, respectively.
The last column lists the total erupted mass calculated based on the corresponding MER figures. Parameters in bold text are also presented in REFIR plots. Empty cell indicates that these values are not computed within REFIR.

MER (kg/s)	Formula	Eq. no.	explicitly used for calculating	Notation in source code	Total erupted mass (kg)
$\boldsymbol{MER_{abs,\min}}$	$Min(MER_1(h_{min}); MER_2(h_{min}); MER_3(h_{min}); MER_4(h_{min}))$		$FMER_{abs,min}$	$Q_{abs.min}$	$\boldsymbol{M_{c\_abs,min}}$
$\boldsymbol{MER_{abs,max}}$	$Max(MER_1(h_{max}); MER_2(h_{max}); MER_3(h_{max}); MER_4(h_{max}))$		$FMER_{abs,max}$	$Q_{abs.max}$	$\boldsymbol{M_{c\_abs,max}}$
$MER_{maxhmin}$	$\mathrm{Max}\ (MER_1(h_{\min}); MER_2(h_{min}); MER_3(h_{min}))$		MER_{lower}; $CMER_{lower}$	$Q_{maxhmin}$	$M_{c\_maxhmin}$
$MER_{maxnowihmin}$	$Min(\ Max\ (MER_1(h_{min}); MER_2(h_{min}); MER_3(h_{min}));\ Min(MER_1(h_{max}); MER_2(h_{max}); MER_3(h_{max})))$		MER_{lower}; $CMER_{lower}$	$Q_{maxnowihmin}$	
MER_{wavg}	$\frac{\sum_{i=1}^{5} w_i MER_i}{\sum_{i=1}^{5} w_i}$	(14)	RMER	Q_{wavg}	
MER_{lower}	$Min(MER_{maxhmin}; MER_{maxnowihmin}; MER_5(h))$		RMER	Q_{lower}	
MER_{upper}	$\frac{\sum_{i=1}^{5} w_i MER_i(h_{max})}{\sum_{i=1}^{5} w_i}$		RMER	Q_{upper}	
RMER	$\frac{MER_{upper}+MER_{wavg}+MER_{lower}}{3}$	(15)	CMER (*)	Q_{RMER}	
$\boldsymbol{CMER_{lower}}$	$Min(MER_{maxhmin}; MER_{maxnowihmin}; MER_5(h); MER_6(h))$		CMER, $FMER_{min}$	Q_{conv_lower}	$\boldsymbol{M_{CMER\_min}}$
$CMER_{wavg}$	$\frac{w_1 MER_{wavg}+w_2 MER_6(h)}{w_1+w_2}$ with $w_{1,2}$ being the *CMER* weight factors	(16)	CMER, FMER	Q_{conv_wavg}	M_{CMER_wavg}
$\boldsymbol{CMER_{upper}}$	$\frac{w_1 MER_{upper}+w_2 MER_6(h_{max})}{w_1+w_2}$ with $w_{1,2}$ being the *CMER* weight factors	(17)	CMER, $FMER_{max}$	Q_{conv_upper}	$\boldsymbol{M_{CMER\_max}}$
CMER	$\frac{CMER_{upper}+CMER_{wavg}+CMER_{lower}}{3}$	(18)	FMER	Q_{CMER}	$\boldsymbol{M_{CMER}}$
$MER_{exp,w\min}$	$\frac{\sum_{i=1}^{4} f_i MER_{expmin,i}}{\sum_{i=1}^{4} f_i}$		$FMER_{min}$, $FMER_{abs,\min}$	Q_{exp_min}	
$MER_{exp,wavg}$	$\frac{\sum_{i=1}^{4} f_i MER_{expavg,i}}{\sum_{i=1}^{4} f_i}$	(19)	FMER	Q_{exp_wavg}	
$MER_{exp,wmax}$	$\frac{\sum_{i=1}^{4} f_i MER_{expmax,i}}{\sum_{i=1}^{4} f_i}$		$FMER_{max}$, $FMER_{abs,\max}$	Q_{exp_max}	
$MER_{man,wmin}$	$\frac{\sum_{i=1}^{N_{man}} a_i MER_{manmin,i}}{\sum_{i=1}^{N_{man}} a_i}$		$FMER_{min}$, $FMER_{abs,\min}$	Q_{man_min}	
$MER_{man,wavg}$	$\frac{\sum_{i=1}^{N_{man}} a_i MER_{manavg,i}}{\sum_{i=1}^{N_{man}} a_i}$	(20)	FMER	Q_{man_wavg}	
$MER_{man,wmax}$	$\frac{\sum_{i=1}^{N_{man}} a_i MER_{man,\ max,i}}{\sum_{i=1}^{N_{man}} a_i}$		$FMER_{max}$, $FMER_{abs,max}$	Q_{man_max}	
$\boldsymbol{FMER_{abs,min}}$	$Min(MER_{abs,\ min}; MER_{exp,\ min}; MER_{man,\ min})$			$Q_{f\_abs.\ min}$	$\boldsymbol{M_{abs,min}}$
$\boldsymbol{FMER_{abs,max}}$	$Max(MER_{abs,\ max}; MER_{exp,\ max}; MER_{man,\ max})$			$Q_{f\_abs.\ max}$	$\boldsymbol{M_{abs,max}}$
$\boldsymbol{FMER_{min}}$	$\frac{a_{conv} CMER_{lower}+a_{exp} MER_{exp,wmin}+a_{man} MER_{man,wmin}}{a_{conv}+a_{exp}+a_{man}}$	(21)		Q_{FMER_min}	$\boldsymbol{M_{FMER\_min}}$
$\boldsymbol{FMER_{max}}$	$\frac{a_{conv} CMER_{upper}+a_{exp} MER_{exp,wmax}+a_{man} MER_{man,wmax}}{a_{conv}+a_{exp}+a_{man}}$	(22)		Q_{FMER_max}	$\boldsymbol{M_{FMER\_max}}$
$\boldsymbol{FMER}$	$\frac{a_{conv} CMER+a_{exp} MER_{exp,wavg}+a_{man} MER_{man,wavg}}{a_{conv}+a_{exp}+a_{man}}$	(23)		Q_{FMER}	$\boldsymbol{M_{FMER}}$

(*): if **PlumeRise** is deactivated.

where the uncertainties Δh_1 and Δh_2 are the error margins of the data sets 1 and 2, respectively.

- if the two data sets are acquired from C-band radar stations and maximum value of the data set with the lower plume height lies below the minimum value of the data set with the higher plume height we consider the data to be *poorly constrained*. The best estimate in this case coincides with the minimum value of the data set that contains the largest plume heights (see Fig. 6b), based on the methodology of retrieving the plume height from a radar scanning at discrete angles (Arason et al., 2011). The uncertainty is calculated using Eq. (2). The situation described above for poorly constrained data might simply be a consequence of the top of the plume height being hidden in a "blind zone", i.e. in a region not covered by the radar.
- if at least one of the data sets is not from a C-band radar sensor but the data sets are disjoint (i.e. non-intersecting), then the data is again considered to be *poorly constrained* (see Fig. 6c). However, in this case the best estimate is determined by calculating the weighted average using the quality factors q_f (see Section 2.4) as weight factors,

$$h_{best} = \frac{q_{f,1}h_1 + q_{f,2}h_2}{q_{f,1} + q_{f,2}} \tag{3}$$

The uncertainty is calculated accordingly, by using the quality factors as weight factors.

4) More than 2 data sets are available ($N > 2$). In this case FOXI.py distinguishes between two cases:

- if the maximum value of the data set with the lowest height is above the overall plume height average and the minimum value of the data set with the highest plume height below the plume height average then the mean value of the plume height data is taken as the best plume height estimate. The range of uncertainty is calculated with Eq. (2), extended to N data sets,

$$s = \left(\frac{1}{N}\sum_{i=1}^{N}\Delta h_i{}^2\right)^{1/2}. \tag{4}$$

- otherwise the best estimate, denoted by h_{best}, is the weighted average of the data using the quality factors (Eq. (3) extended to N data sets). The range of uncertainty Δh_{best} is given by:

$$\Delta h_{best} = h_{best} - h_{w,\,min} \tag{5}$$

where $h_{w,min}$ represents the quality-factor weighted average of the minimum plume heights in each data set, denoted by $h_{min,i}$ for data set i, so that

$$\frac{h_{w,\,min} = \sum_{i=1}^{N} q_{f,i}h_{\,min}, i}{q_{f,i}} \tag{6}$$

This procedure has been designed to guarantee the most reliable value of the plume height h based on the available data. As a result of the procedure applied by FOXI, h can significantly vary, based on the selected time base (see Section 5.2 for strategies).

Table 4
Overview of the scenarios tested by REFIR.

	Scenario I		Scenario II		Scenario III a-c		
Eruption (day)	Hekla 2000 (26/27 Feb 00)		Eyjafjallajökull 2010 (6 May 10)		Eyjafjallajökull 2010 (6 May 10)		
Weight factors in Eq. (13) w_1: w_2: w_3: w_4: w_5	1: 1: 1: 1: 1		1: 1: 1: 1: 1		1: 1: 1: 1: 1		
Simulation time (h:min)	00:00–05:43	05:44–10:00	00:00–12:00	12:01–24:00	00:00–01:00	01:01–01:41	01:42–03:00
Selected time base	15 min		15 min		Scenario IIIa: 15 min Scenario IIIb: 30 min Scenario IIIc: 60 min		
Remark	1)	2)	3)	4)	5)	data gap	6)
ISKEF data	Yes[a]	Yes[a]	Yes[a]	Yes[a]	Yes[a]	–	Yes[a]
ISEGS data	–	–	–	–	–	–	–
ISX1 data	Yes[b]	Yes[b]	Yes[b]	Yes[b]	Yes[b]	–	Yes[b]
ISX2 data	Yes[b]	Yes[b]	Yes[b]	Yes[b]	Yes[b]	–	Yes[b]
CAM 1 data	Yes[b]	Yes[b]	–	–	–	–	–
CAM 2 data	Yes[b]	Yes[b]	–	–	–	–	–
CAM 3 data	Yes[b]	Yes[b]	–	–	–	–	–
Plume width (km)	0.4–0.6		1–1.5		1–1.5		
P_0 (Pa)[c]	84,076		82,409		82,409		
T_0 (K)	266	265	281	275	275		
w (m/ s)	10	8.5	9.8	14.4	14.4		
ΔT (K m^{-1})	−0.0070	−0.0067	−0.00607	−0.00628	−0.00628		
$H_{tropopause}$ (km)	9.0	8.5	12.5	11.8	11.8		
$H_{stratosphere}$ (km)	18.0		18.0		18.0		

Remarks:
Plume height and atmospheric data used are based on measured conditions on:
1) 26/2/2000, 18:17–24:00 UTC.
2) 27/2/2000, 00:00–04:00 UTC.
3) 6/5/2010, 00:00–12:00 UTC.
4) 6/5/2010, 12:00–00:00 UTC.
5) 6/5/2010, 12:00–13:00 UTC.
6) 6/5/2010, 13:35–15:00 UTC.
[a] Measured data.
[b] Simulated data.
[c] P_0: Ambient atmospheric pressure at the vent.

3.2. Calculation of the mass eruption rate

3.2.1. Mass eruption rate from simplified models

3.2.1.1. Models used by REFIR. During eruptions, availability of data can vary from, for example, only manual observations of plume height to continuous data streams from a variety of sensors on both plume and atmospheric conditions. REFIR is constructed to be of near-real time operational use in all situations, including cases of limited data. Hence, as well as having the option of more sophisticated methods for MER estimate, it makes use of simplified empirical relationships and semi-empirical or theoretical 0D and 1D models. Despite their simplifications, numerous studies have demonstrated that these models work reasonably well (Costa et al. 2016), suggesting that the underlying assumptions are useful for the volcanic plume case.

Five 0D plume models are implemented in FOXI. Additionally, a 1D model may be added, using an external server. The 0D models adopted are:

- **"Wilson Walker"**: 0D theoretical model by Wilson and Walker (1987) in which the MER is estimated as

$$MER_1 = \left(\frac{h}{c}\right)^4 \tag{7}$$

where h is the plume height above the vent, and c is a dimensional fitting constant (with value 236 $m(s/kg)^{1/4}$, calculated based on data fitting). This model is originally developed to describe central, silica-rich, Plinian eruptions with an eruption column that is not influenced by a cross wind.

- **"Sparks"**: 0D empirical model by Sparks (1997) where the MER is estimated as

$$MER_2 = \rho\left(\frac{h}{c}\right)^{3.86} \tag{8}$$

where ρ is the dense rock equivalent density of the erupted magma and c is a dimensional constant (with value 1670 $m(s/m^3)^{1/3.86}$).

- **"Mastin"**: 0D empirical model by Mastin et al. (2009) where the MER is estimated as

$$MER_3 = \rho\left(\frac{h}{c}\right)^{4.15} \tag{9}$$

where ρ is 2500 kg/m^3 and c is a dimensional constant (with value 2000 $m(s/m^3)^{1/4.15}$, calculated based on data fitting)

- **"Gudmundsson"**: 0D empirical model by Gudmundsson et al. (2012) where the MER is estimated as

$$MER_4 = \rho a k_l \left(\frac{h_{avg} + h_{max}}{c}\right)^{4.15} \tag{10}$$

where h_{avg} and h_{max} are the average and maximum plume heights, respectively, c is the same constant as for "Mastin", a is a dimensionless

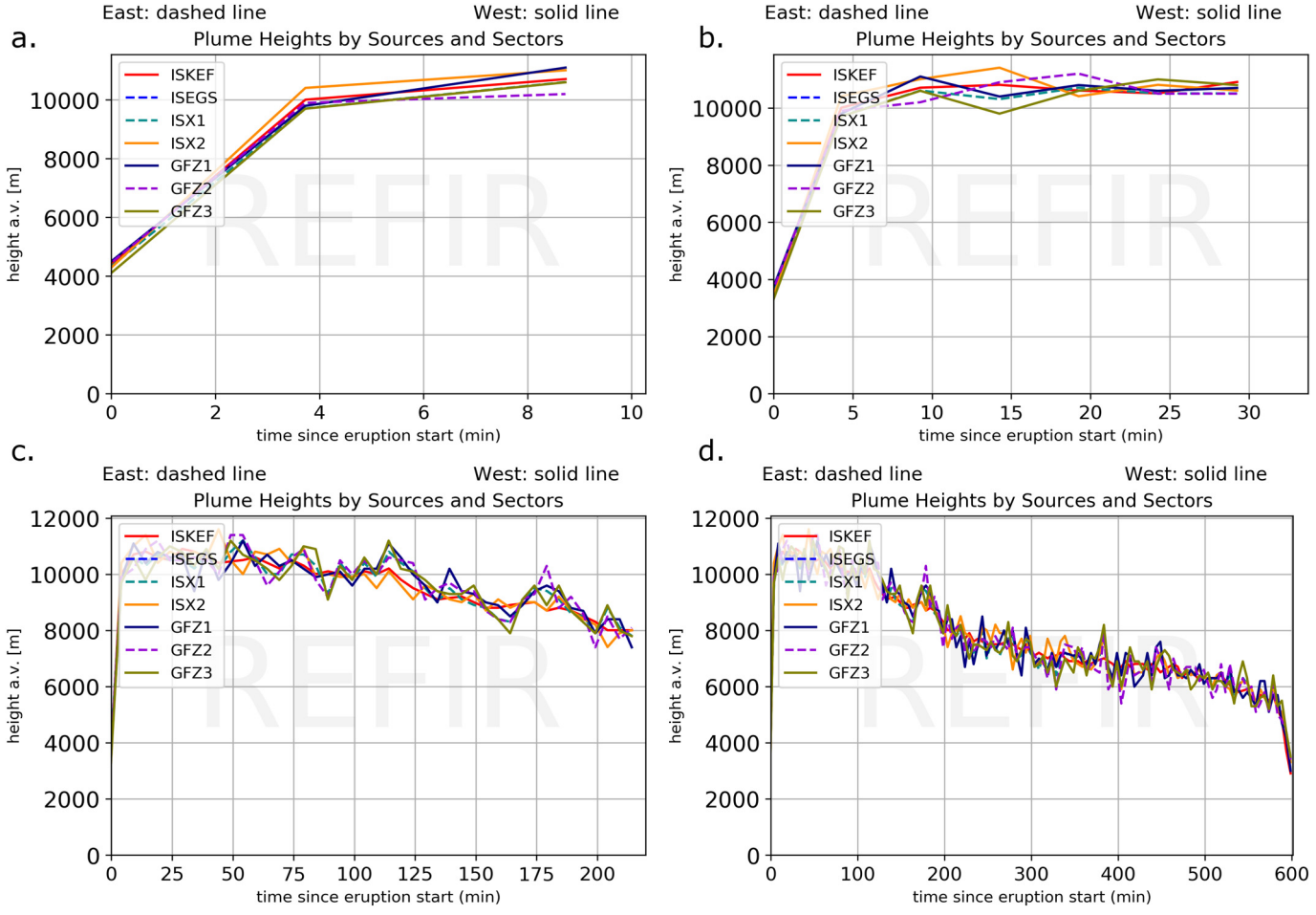

Fig. 8. Scenario I – Hekla 2000: Plot sequence showing plume heights above vent as measured with different sensors. This test case simulated the formation of a short-lived sub-Plinian ash column, similar to the evolution of the ash plume occurring during the Hekla 2000 eruption. Screenshots show the plots provided by FOXI.py after 10 (a), 30 (b), 220 (c) and 600 (d) minutes.

constant which is calibrated to be 0.0564. k_l is a scaling factor which was found to be 2.15 for the first (phreatomagmatic) stage (14–16 April) of the Eyjafjallajökull 2010 eruption. For the subsequent magmatic eruption phases k_l dropped to 1.58 for 17 April and 1.59 for 18 April – 22 May (see Gudmundsson et al., 2012). In REFIR, k_l can be assigned manually by the operator via the graphical user interface FIX.py.

- **"modified Degruyter Bonadonna"**: an adapted approach using the 0D theoretical model by Degruyter and Bonadonna (2012), which is based on both Morton et al. (1956) and Hewett et al. (1971) in order to take into account the effect of various eruptive and atmospheric features including magma temperature, wind, advection and atmospheric stratification, where the MER is estimated as

$$MER_5 = \pi \frac{\rho_{a0}}{g'} \left(\frac{2^{5/2} \alpha^2 \overline{N}^3}{z_1^4} H^4 + \frac{\beta^2 \overline{N}^3 \overline{v}}{6} H^3 \right), \quad (11)$$

where H is the maximum height of the centerline of the plume above the vent (see Fig. 7), $\overline{N}$ is the average buoyancy frequency of the atmosphere (measured in 1/s), $\overline{v}$ the wind velocity averaged across the plume height (measured in m/s), ρ_{a0} is a reference density for the surrounding atmosphere (measured in kg/m^3), g' is measured in m/s^2 and defined as $g \cdot ((c_0\theta_0 - c_{a0}\theta_{a0})/c_{a0}\theta_{a0})$ with g being the gravitational acceleration, c_0 and θ_0 being the source specific heat capacity and temperature of the plume and c_{a0} and θ_{a0} being the heat capacity and temperature of the surrounding atmosphere; α and β are the dimensionless radial and wind entrainment coefficients, respectively, and z_1 (=2.8) is the maximum non-dimensional height determined by numerical integration of the non-dimensional governing equations described in *Morton* et al. (1956). For a detailed description on these parameters, the reader is referred to Degruyter and Bonadonna (2012).

We note that this model gives the mass eruption rate as a function of the plume centerline height H instead of the plume top height h. Although cases have been reported where this difference is a minor factor (Bonadonna et al., 2015; Marzano et al., 2016), in theory this would mean that, if h as obtained with the procedure explained above is used in Eq. (11) as an approximation of H, this approach might overestimate MER in case of bent-over plumes. In order to correct for this possible effect, FOXI.py first classifies the plume as vertically evolving or bent-over by computing the parameter Π (Degruyter and Bonadonna, 2012) defined as

$$\Pi = 6 \frac{2^{5/2}}{z_1^4} \frac{\overline{N} h}{\overline{v}} \left(\frac{\alpha}{\beta} \right)^2. \quad (12)$$

According to theory, the two different end members of plume types are characterized by $\Pi >> 1$ and $\Pi << 1$, respectively. However, to date, a single threshold value, required for discriminating between the two scenarios in operational use, has not been defined and is likely to be case-specific. By default, REFIR uses a threshold value of 5 to discriminate between the two plume types. We note, however, that this threshold is just a suggestion and probably has to be calibrated to the specific volcano. The threshold value of Π can be easily modified by changing the value for the parameter PI_THRESH in the settings section of the FOXI.py source code.

Hence, if $\Pi > 5$ then the plume motion is assumed to be predominantly vertical; otherwise the plume is treated to be bent over. In the former case, the difference of h and H is considered to be negligible and Eq. (11) is computed with the best estimate of plume height h. In the latter case, FOXI.py uses this model only if the half-width of the plume (radius) r is available, in which case H in Eq. (11) can be approximated to be $H = h - r$. The plume half-width parameter can come either from observations (FIX.py allows the operator to manually enter values for the plume width $2r$), or from simulations with a 1D plume model that the user can optionally activate (see **PlumeRise** below). If r is not available, the **modified Degruyter Bonadonna** approach is deactivated. Hence for making sure this 0D model is included,

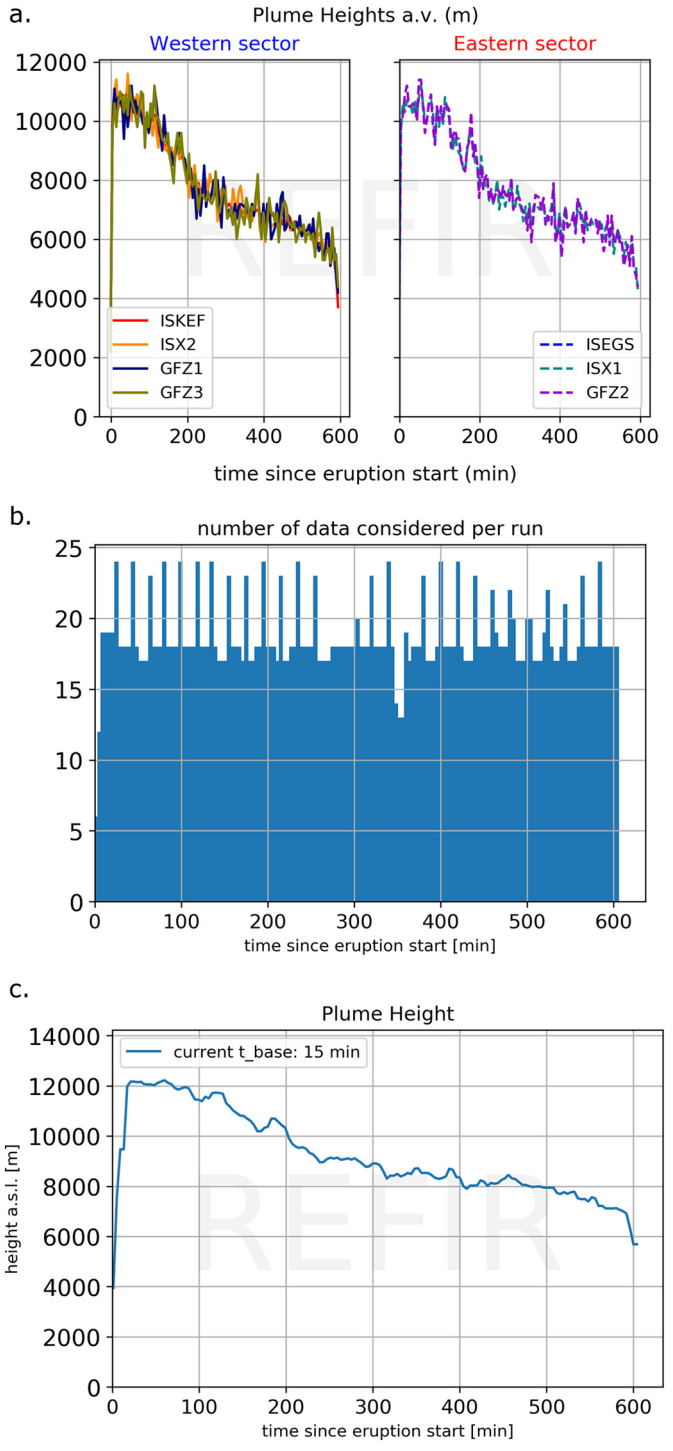

Fig. 9. Scenario I – Hekla 2000, simulated data stream by six sensors: (a) plume height sector plot, (b) N-plot and (c) the plot displaying the constrained plume height. The latter plot, in contrast to the other plume height plots produced by REFIR, provides absolute plume height values above sea level (a.s.l.), not above vent (a.v.). It presents the result of the first data processing level (see also Section 2.4 and Fig. 5, green box) which was in the next step converted to height above vent h and then used as input parameter for the plume models integrated in REFIR.

it is important for the operator to define a plume width $2r$ (see Section 5.3 for strategies). It is noted here that we call this approach "modified Degruyter Bonadonna", to avoid confusion with the original strategy used by the developers of the underlying model (e.g., Degruyter and Bonadonna 2012, Bonadonna et al. 2015, Marzano et al. 2016).

- **"PlumeRise"**: 1D integral model by Woodhouse et al. (2013), which takes into account the effect of wind. This model is not included in FOXI.py but can be optionally activated by the user and run on an external server where the PlumeRise model calculations are performed. The estimate provided by PlumeRise is denoted MER_6. The PlumeRise calculations are conducted with recent meteorological data suitable for the ongoing eruption. For the purpose of data intercommunication, FOXI.py generates a file, called "Foxi_hbe.txt", and exports it to an online accessible server. In addition to a time stamp and information on the volcano of interest (including vent height), it mainly contains the range of plume heights estimated by FOXI. This data is then imported by a PlumeRise/FOXI interface located and operated by University of Bristol, using the plume height data to determine a best MER estimate computed by the numerical model PlumeRise for a wide range of source conditions (magmatic temperature, gas mass fraction, vent radius etc.). For details on the equations and the numerical method, the reader is referred to Woodhouse et al. (2013). The resulting MER values and predictions on the current plume diameter are then exported via a text file named "PlumeRise_out.txt" and imported into FOXI.

In the current version of REFIR, the PlumeRise/FOXI interface can only be run in the "FutureVolc setup", since it utilizes meteorological

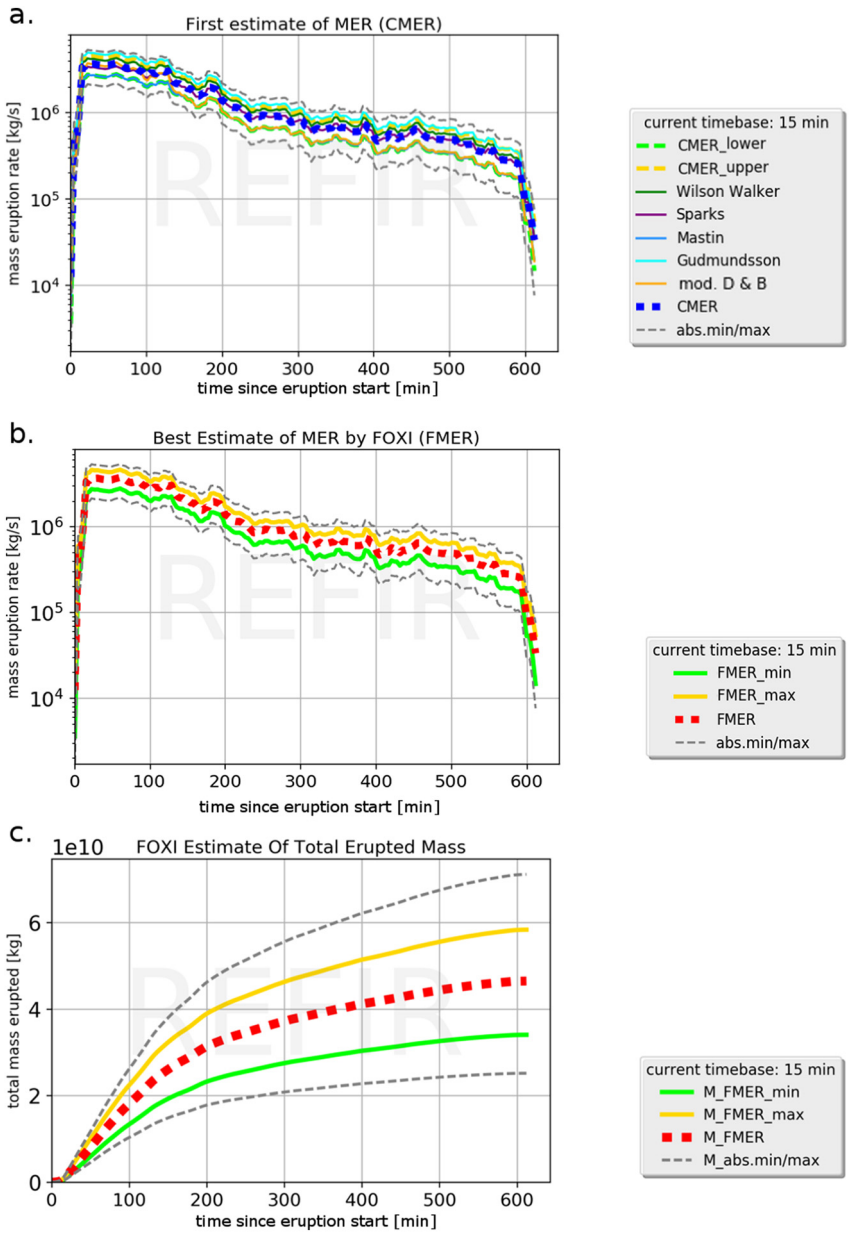

Fig. 10. Scenario I – Hekla 2000, simulated data stream by six sensors. Plots of (a) CMER, (b) FMER and (c) total mass as a function of time, as provided by FOXI. CMER (bold dashed blue line) stands for the mass eruption rate estimated with up to six conventional models. The conclusive best estimate provided by FOXI.py is FMER (dashed red line), plotted along with its predicted range of uncertainty. Bottom plot shows the total erupted mass, estimated for scenario I, finally ranging from 3.4×10^{10} kg to 5.8×10^{10} kg.

data collected routinely by radiosonde at Keflavik and streamed from IMO to the PlumeRise server twice daily, ensuring a suitable atmospheric sounding is available in the model. Further refinement of the atmospheric data can be achieved by atmospheric soundings proximal to the volcano. In principle meteorological data from locations outside Iceland could be used, e.g. from radiosonde soundings made at meteorological stations around the world. However, in some regions these soundings may not always be available. Further refinement of the PlumeRise interface to the REFIR system is currently in preparation to provide global access to the PlumeRise model.

3.2.1.2. First step: computation of MER by REFIR-internal 0D models (RMER). Based on the individual MER estimates resulting from the 0D models listed above, a set of values are obtained by using the complete range of variation of the assessed observed plume height (h, h_{min} and h_{max}). These parameters are used to calculate a statistically robust range of solutions for MER, here called RMER (REFIR-internal models MER). Table 3 lists all formulas computed by REFIR. In the following we present only the core equations, crucial for the understanding of the REFIR strategy. For details on individual procedural steps and calculations we refer the reader to the companion manual (supplement S2).

REFIR follows the strategy of applying weighed averages at each data processing level (see Section 2.4). Hence as a first step, the weighted average of all MER values (MER_{wavg}) is obtained by applying the average best estimate of the plume height h and using the model-specific weight factors w_i. These allow the operator to give a specific weight to each model, hence letting some model outputs be more influential on the final MER estimate. MER_{wavg} is calculated as:

$$MER_{wavg} = \frac{\sum_{i=1}^{5} w_i MER_i}{\sum_{i=1}^{5} w_i}. \quad (13)$$

Next to the lowest and highest extreme of all MER estimates ($MER_{abs,min}$ and $MER_{abs,max}$), REFIR provides the RMER as well as a preliminary estimate for the lower and upper constraints:

- MER_{lower}: the minimum of the three values given by $MER_{maxhmin}$, $MER_{maxnowihmin}$ and by the wind-affected model from **modified Degruyter Bonadonna** (if activated), using the plume height estimate h. Therein, $MER_{maxnowihmin}$ and $MER_{maxnowihmin}$ are statistically derived parameters based on criteria specified in Table 3.
- MER_{upper}: weighted average of all MER values obtained by applying the maximum plume height h_{max}:

$$MER_{upper} = \frac{\sum_{i=1}^{5} w_i MER_i(h_{max})}{\sum_{i=1}^{5} w_i} \quad (14)$$

- *RMER*: "best estimate" by FOXI using the activated REFIR-internal 0D models:

$$RMER = \frac{MER_{upper} + MER_{wavg} + MER_{lower}}{3}. \quad (15)$$

3.2.1.3. Second step: Computation of conventional MER (CMER). If **PlumeRise** is activated, REFIR incorporates the maximum, average and minimum estimate of *MER* as obtained by this 1D model and recalculates all the key values listed above accordingly. MER_{wavg} and MER_{upper} are updated to include the new values by means of two additional weight factors defined by the operator, one related to the 0D (w_{1-5}) and the other to the **PlumeRise** model (w_6). We call the resulting values conventional MER (CMER):

- $CMER_{lower}$: the minimum of the four values given by $MER_{maxhmin}$, $MER_{maxnowihmin}$ and by the two wind-affected models from **modified Degruyter Bonadonna** and **PlumeRise**, both using the plume height estimate h.
- $CMER_{wavg}$:

$$CMER_{wavg} = \frac{w_{1-5} MER_{wavg} + w_6 MER_6(h)}{w_{1-5} + w_6}. \quad (16)$$

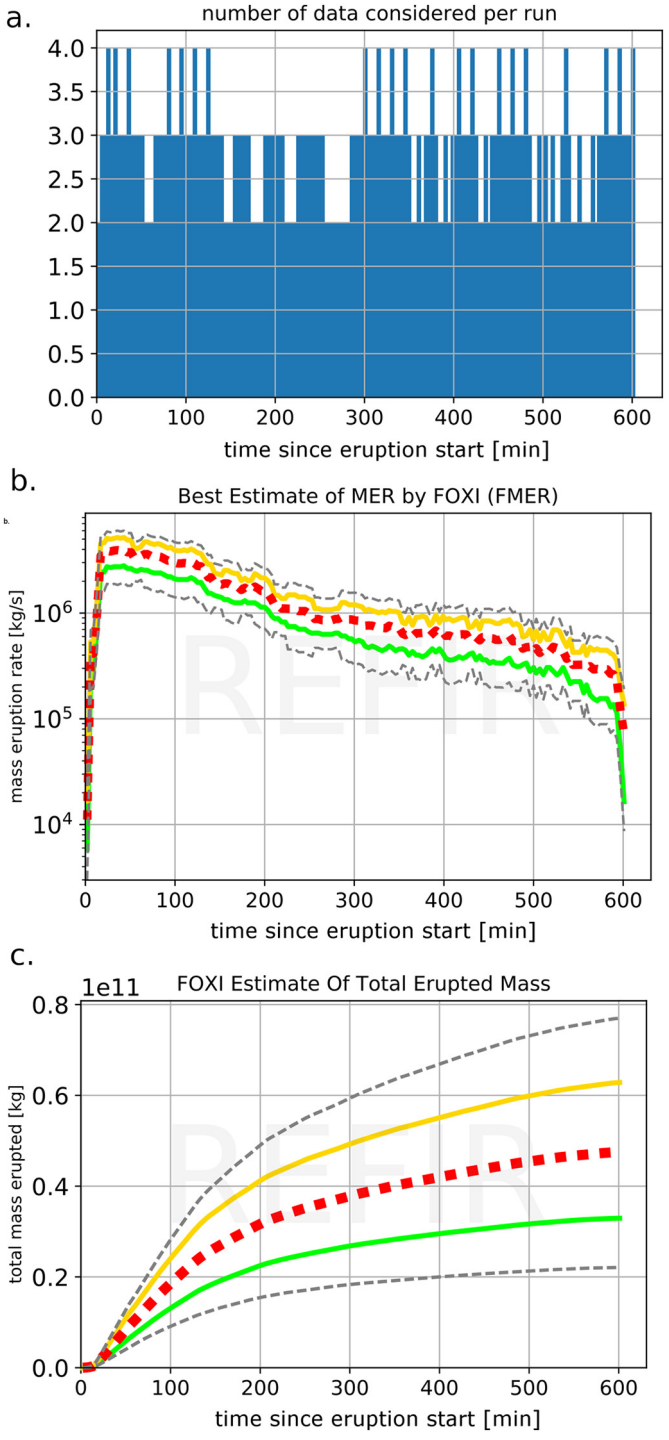

Fig. 11. Scenario I –Hekla 2000: resulting plots of simulation, this time with measured data provided exclusively by ISKEF. The reduced number of data streamed to FOXI.py are reflected by the N-plot (shown in a). It resulted in an increased range of uncertainty for the estimated FMER (shown in b) and consequently also in that for the erupted mass (shown in c). FOXI.py estimates the overall mass erupted during the 10 h scenario to be in a range from 3.3×10^{10} kg to 6.3×10^{10} kg.

- $CMER_{upper}$:

$$CMER_{upper} = \frac{w_{1-5} MER_{upper} + w_6 MER_6(h_{max})}{w_{1-5} + w_6}. \quad (17)$$

The final CMER value is then calculated as

$$CMER = \frac{CMER_{upper} + CMER_{wavg} + CMER_{lower}}{3} \quad (18)$$

If **PlumeRise** is deactivated, $CMER_{upper}$, $CMER$ and $CMER_{lower}$ are simply set equal to $RMER_{upper}$, $RMER$ and $RMER_{lower}$.

3.2.2. Mass eruption rate from experimental sensors

FOXI.py offers the possibility to include MER estimates by four independent alternative data sources (here referred to as experimental sensors): infrasound (Ripepe et al., 2013), electric field (Büttner et al., 2000), pulse analysis (Dürig et al. 2015b) and radar scattering (Marzano et al., 2016). We note that these four methods are just suggestions. Each of them can be easily replaced by any other external measurement routine that provides MER and uncertainties in near real-time, regardless if it is based on near-field or remote sensing (e.g., from satellites). The influence of the individual experimental sources on the MER estimate can be regulated by operator-defined weight factors f_i, similarly to the weighting of plume models. FOXI.py first computes the average MER value for each sensor $MER_{expavg,i}$ and

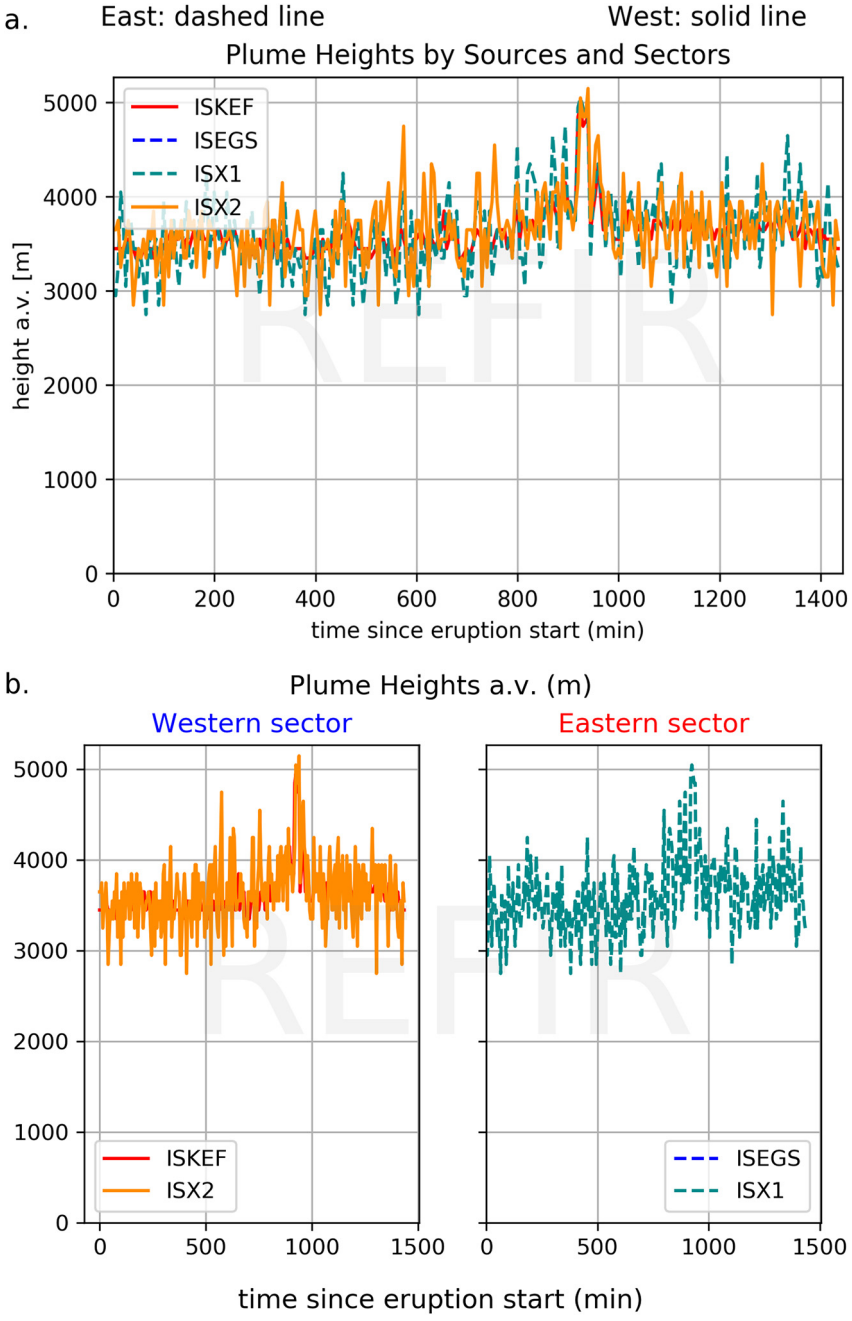

Fig. 12. Scenario II – Eyjafjallajökull 2010: Plume heights plotted by the individual sources (a). No significant difference between the Eastern and the Western sector was simulated, as it can also be seen in the plume height sector plot (b).

finally calculates the best estimate of MER, $MER_{exp,wavg}$ by a weighted averaging of all the $MER_{expavg,i}$,

$$MER_{exp}, wavg = \frac{\sum_{i=1}^{4} f_i MER_{expavg,i}}{\sum_{i=1}^{4} f_i}. \quad (19)$$

The same equation is applied to the minimum and maximum values from the experimental sensors in order to obtain the maximum and the minimum estimate of MER_{exp}: $MER_{exp,wmax}$, $MER_{exp,wmin}$. Equations for conversion of signal to MER are not given here and these data sources are not considered further.

3.2.3. Importing manually added mass eruption rate estimates

If available, the operator can add N_{man} data sets of MER estimates (minimum $MER_{min,i}$ and maximum $MER_{max,i}$) manually, together with weight factors a_i. FOXI.py first computes the average MER manual $MER_{manavg,i}$ and finally calculates the best estimate of the manually added MER, $MER_{man,wavg}$, as a weighted average of all the $MER_{manavg,i}$,

$$MER_{man,wavg} = \frac{\sum_{i=1}^{N_{man}} a_i MER_{manavg,i}}{\sum_{i=1}^{N_{man}} a_i}. \quad (20)$$

The same equation is applied to the minimum and maximum values from the manually added estimates in order to obtain the maximum and the minimum estimate of MER_{man}: $MER_{man,wmax}$, $MER_{man,wmin}$. In addition, the average weight factor a_{man} for the manually added MER is calculated.

3.2.4. Calculation of the final best mass eruption rate estimate (FMER)

In this final step, FOXI.py computes the conclusive "Final best MER estimate" (FMER) by merging the conventional (CMER), and, if applicable, experimental sensor derived and manually added MER estimates. In addition, at this stage the operator can specify weight factors for the first two components (a_{conv}, a_{exp}); for the manually added MER, the weight factor a_{man} is computed by FOXI.py as explained above. FOXI.py defines ranges of variations together with the best estimate. The resulting five key values represent the main output of REFIR and are defined as follows:

- $FMER_{abs,min}$: is the lowest possible value of MER calculated as the minimum of $MER_{abs,min}$, $MER_{exp,min}$ and $MER_{man,min}$.
- $FMER_{abs,max}$: is the highest possible value of MER calculated as the maximum of $MER_{abs,max}$, $MER_{exp,max}$ and $MER_{man,max}$.
- $FMER_{min}$: the lower boundary of the range of best MER estimates (FMER) calculated as

$$\frac{FMER_{min} = a_{conv} CMER_{lower} + a_{exp} MER_{exp}, wmin + a_{man} MER_{man,wmin}}{a_{conv} + a_{exp} + a_{man}}. \quad (21)$$

- $FMER_{max}$: the upper boundary of the range of best MER estimates (FMER) calculated as

$$FMER_{max} = \frac{a_{conv} CMER_{upper} + a_{exp} MER_{exp,wmax} + a_{man} MER_{man,wmax}}{a_{conv} + a_{exp} + a_{man}}. \quad (22)$$

- $FMER$: the average best MER estimate calculated as

$$\frac{FMER = a_{conv} CMER + a_{exp} MER_{exp}, wavg + a_{man} MER_{man,wavg}}{a_{conv} + a_{exp} + a_{man}} \quad (23)$$

3.3. Calculation of the total erupted mass

FOXI.py calculates the total erupted mass, denoted by M, based on the $CMER$ and $FMER$ best estimates and the minimum and maximum values by integrating over the total time since the start of the eruption, denoted by te,

$$M = \int_0^{te} MER(t)dt \quad (24)$$

In particular, FOXI.py performs this integration for any estimate of MER obtained with the different models and/or data source. The whole set of mass estimates provided by FOXI.py is summarized in Table 3.

4. Test scenarios – examples for REFIR results

In order to demonstrate the functionality of REFIR and its capability to handle multiple sensors, different types of data streams and data gaps, we performed simulations of eruptive scenarios based on plume height records measured by the C-band radar station at Keflavík (ISKEF), which was the only applicable source of plume height information for the periods in question.

For this purpose we have simulated data for several sensors based on this single real data stream. Three scenarios are based on observations made during specific periods of the eruptions of Hekla in 2000 and Eyjafjallajökull in 2010. Table 4 summarizes the input parameters used for the three scenarios. The periods simulated are:

- 26/27 February 2000, when Hekla volcano entered a short-lived explosive phase, forming a sub-Plinian eruptive column. (Lacasse et al., 2004; Höskuldsson et al., 2004; Soosalu et al., 2005).
- 6 May 2010 during the Eyjafjallajökull eruption (Arason et al., 2011;

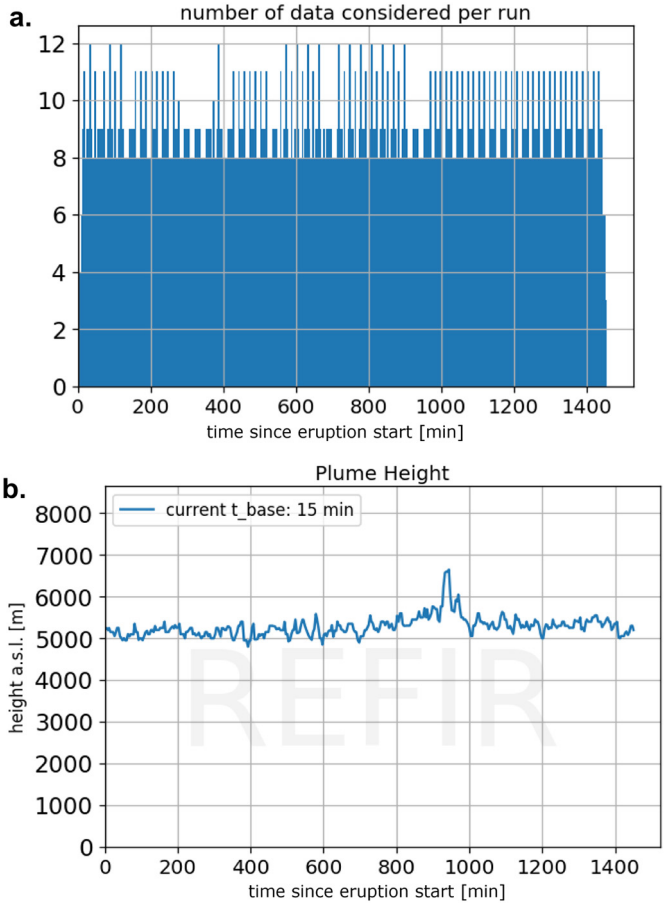

Fig. 13. Scenario II – Eyjafjallajökull 2010: (a) N-plot and (b) estimated plume height. Except for a slight increased plume height at ~960 min, the top of the ash plume remained at a relatively constant altitude.

Dellino et al., 2012; Gudmundsson et al., 2012; Bjornsson et al., 2013). The explosive phase of this eruption started on 14 April and lasted for 39 days. It had a first phreatomagmatic phase of four days followed by a phase of weaker activity. The eruption entered a third, explosive, mostly magmatic phase on 5 May. The situation on 6 May selected for simulation represents a part of a long-lived explosive magmatic eruption forming a wind-affected sustained eruption column.

All runs were performed in real time by simulating plume height data streams of the active sensors (see Table 4) with a time interval of 5 min. For each of these simulations, all five REFIR-internal 0D models were used and equally weighted (using the default setting as shown in Fig. 3a). The atmospheric parameters were selected according to radiosonde measurements in Keflavik on the respective days (data archive: http://weather.uwyo.edu/upperair/sounding.html). All output files generated by REFIR can be found in supplement S3.

The simulations performed may not reflect the local conditions in every detail. They serve the purpose to demonstrate the potential of REFIR as a real-time monitoring system. Although based on the real events, most of the plume height data used were simulated (not measured) since most of the presented data sources have not been installed by that time, and the only available C-band radar data is fragmentary. The simulated sensors were presumed to be optimally located. In addition, some of the assumptions might deviate from the actual historic situation.

4.1. Simulated scenario I: Hekla 2000 (26/27 February 2000)

Plume height data was simulated based on the first 10 h of the radar recordings from ISKEF described in Lacasse et al. (2004), beginning with the onset of the explosive eruption at 18:17 UTC on February 26. On the basis of these recordings, fictional data-streams for additional five sensors (ISX1, ISX2, CAM1, CAM2, CAM3 see also Table 4) were generated by adding noise in form of normally distributed random numbers to the values from ISKEF (using a standard deviation of 0.5 km and a mean value of 0). The simulated visibility is completely fictitious and does not reflect the (in fact very poor) visibility situation in the night of 26/27 February 2000. Note that we also simulate data streams provided by the auto-tracking web cameras when in reality visual-light

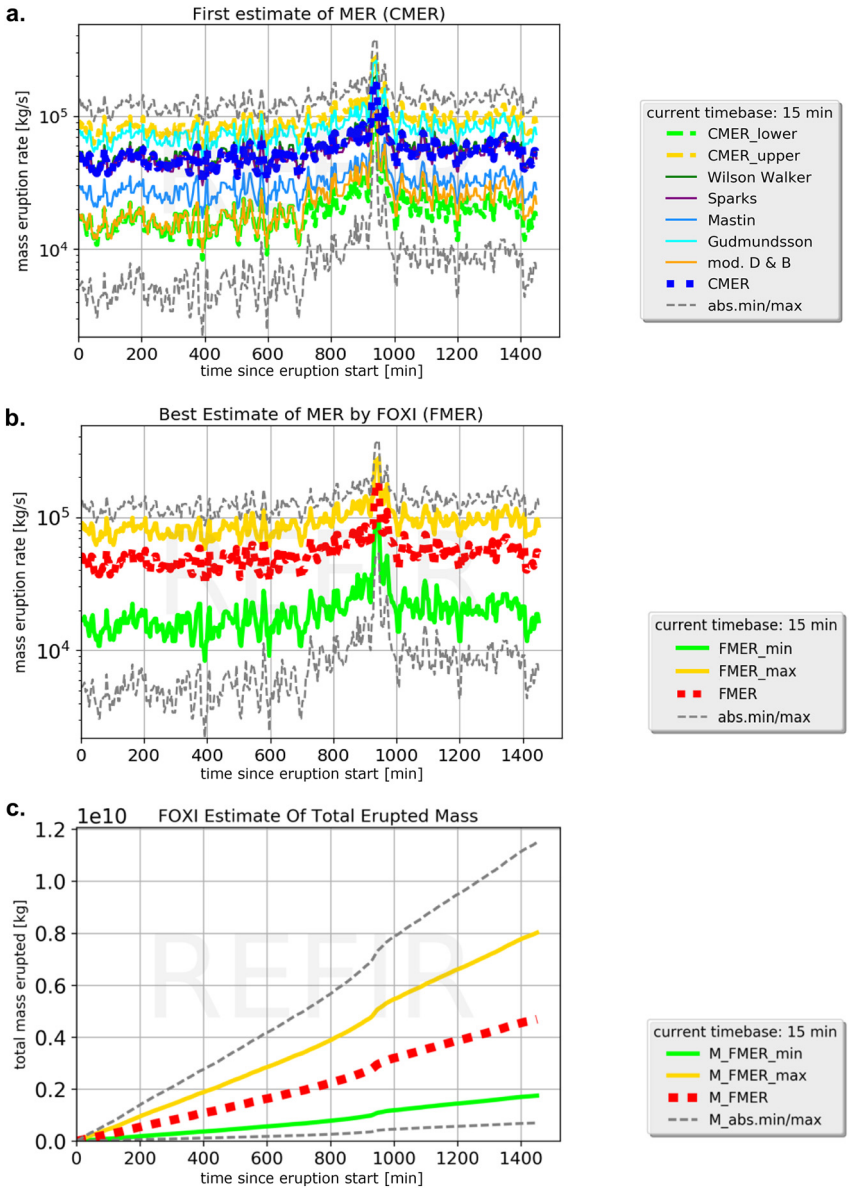

Fig. 14. Scenario II – Eyjafjallajökull, 2010: (a) CMER and (b) FMER as functions of time. Since all included plume models depend on the plume height, the peak at ~960 min resulted in a significant increase in the estimated mass eruption rate. Plot (c) shows the total mass erupted as a function of time for the 24 h of the simulation.

cameras would be ineffective at night. The series from all sensors for which data were simulated can be found in supplement S3, under "scenario_I".

Fig. 8 presents a sequence of screenshots of REFIR outputs at runtime; in particular, the plume height (measured above the vent) recordings from different sensors are displayed as a function of time. In this simulation, all data sources contribute except for ISEGS, which was deactivated. In this scenario, the top of the plume quickly reached a level of 11 km above the vent (which was in this simulation assumed to be situated 1491 m above sea level) and subsequently declined slowly. For this test run, a time base of 15 min was selected, in order to monitor the plume evolution with the highest possible temporal resolution. In Fig. 9a a "plume height sector plot" is presented, for which data is segregated based on the location of the data sources. This type of plot allows the system operator to identify and analyze possible East/West wind-distortion of the ash column monitored, which reflects the predominant wind directions in Iceland. In the case shown, the plume heights measured by sensors located in the west of Hekla are very similar to those measured in the eastern sector, implying that in this scenario no wind-distortion was simulated.

Fig. 9b shows an "N-plot", illustrating the temporal evolution of the number of plume height data points that were considered by FOXI.py for computing the best estimate and the mass eruption rate. This plot can serve as indicator of how reliable the estimate of REFIR has been at a given time. As a rule of thumb, it can be assumed that the lower the number of data available, the lower the expected accuracy of plume height and MER estimate. In the scenario, the number of data considered by FOXI.py clearly decreased for a short time at approximately 360 min after the beginning of the simulation. However, the 13 measurement points in this period of reduced data can still be considered to be comprehensive and therefore a reliable statistical basis in view of experiences made in real eruptions (Arason et al., 2011; Oddsson et al., 2012; Gudmundsson et al., 2015), and justifies the use of the shortest time base possible within REFIR (15 min). The plot presented in Fig. 9c displays the best estimate of plume height above sea level, computed by FOXI.py on the basis of the individual plume height data sets. The curve represents the result of processing level 1 (see Section 3.1 and Fig. 5). This estimate is then converted into plume height above vent h, which is used as an input parameter for the plume models. The results for MER and CMER from the plume models are displayed in Fig. 10a. Since no additional MER data by external systems was provided, the conclusive best estimate for mass eruption rate (FMER) is identical to the CMER, as shown in Fig. 10b.

The total mass erupted based on the FMER estimations is displayed in Fig. 10c. Hence, after 10 h, the total erupted mass has been estimated to be between 3.4×10^{10} kg and 5.810^{10} kg. This is 3–6 times higher than the estimated tephra deposit (Haraldsson, 2001), but as this eruption was also producing lava, some energy from, e.g., vigorous fire fountains may have contributed to the buoyant rise of the plume, thus leading to an overestimate of the MER by the applied models.

Feeding FOXI.py exclusively with the data that was actually measured (provided by the C-band radar station ISKEF as a single source), results in larger uncertainties of CMER and FMER (see Fig. 11b). This is reflected in the final estimate for the overall erupted mass, which is found to be between 3.3×10^{10} kg and 6.3×10^{10} kg (see Fig. 11c). Thus, in comparison to the multi-sensor simulation, the range of

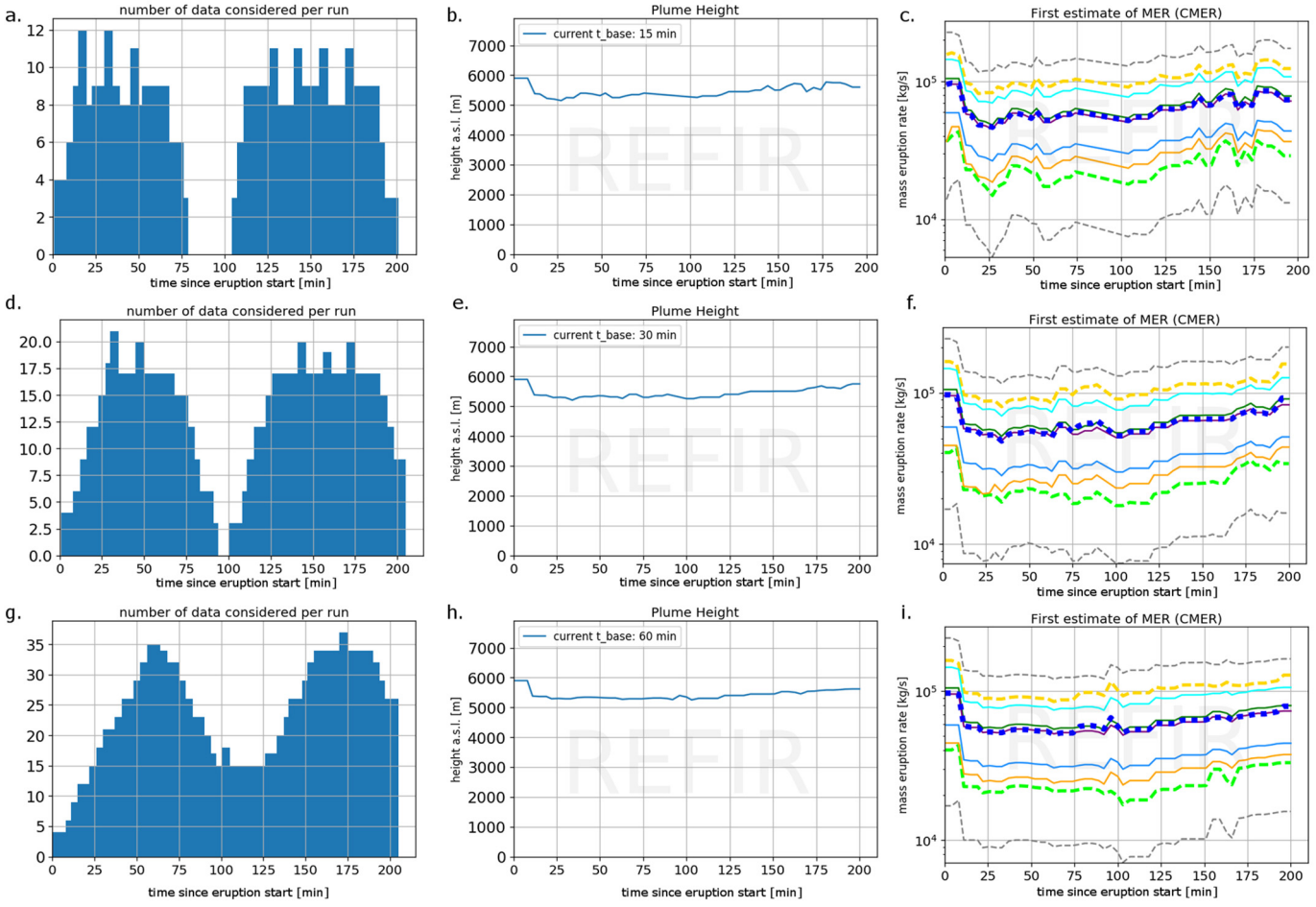

Fig. 15. Scenario II – Eyjafjallajökull, 2010: Resulting plots at the end of the 3 h simulation of scenario III. N-plots (left column), computed plume heights (center column) and CMER plots (right column, for legend see, e.g., Fig. 10 a.) are presented. The individual rows present the FOXI.py outputs with a selected time base of (top row) scenario IIIa, 15 min; (middle row) scenario IIIb, 30 min; (bottom row) scenario IIIc, 60 min.

Table 5
Total erupted mass computed on the basis of Scenario III for three different time bases. For comparison, the maximum deviation between the results is presented (column 6) and referred to the highest of the three values (column 7).

1	2	3	4	5	6	7
Time after scenario start	Time base	Scenario IIIa	Scenario IIIb	Scenario IIIc	Max deviation	Relative max deviation
		15 min	30 min	60 min		
	SI unit	kg	kg	kg	kg	%
63 min	M_{CMER_min}	8.6×10^7	9.2×10^7	9.5×10^7	8.9×10^6	9.3
	M_{CMER}	2.2×10^8	2.2×10^8	2.3×10^8	7.4×10^6	3.2
	M_{CMER_max}	3.8×10^8	3.7×10^8	3.8×10^8	1.1×10^7	3.0
122 min	M_{CMER_min}	1.6×10^8	1.6×10^8	1.7×10^8	1.1×10^7	6.5
	M_{CMER}	4.2×10^8	4.3×10^8	4.3×10^8	6.5×10^6	1.5
	M_{CMER_max}	7.3×10^8	7.3×10^8	7.2×10^8	4.7×10^6	0.6
181 min	M_{CMER_min}	2.6×10^8	2.6×10^8	2.6×10^8	2.4×10^6	0.9
	M_{CMER}	6.7×10^8	6.7×10^8	6.6×10^8	1.5×10^7	2.2
	M_{CMER_max}	1.2×10^9	1.1×10^9	1.1×10^9	3.5×10^7	3.1

uncertainty increased by 0.6×10^{10} kg. In other words, using additional data from various sources would in this case decrease the uncertainty by 25%. This example demonstrates that, provided the data delivered is consistent, increasing the number of independent data sources by adding sensors is an important element for increasing the accuracy of the estimates and narrowing the uncertainty.

4.2. Simulated scenario II: 24 h during the Eyjafjallajökull 2010 eruption (6 May 2010)

In this simulation, 24 h of C-band radar data, including some data gaps were used, originally recorded by ISKEF on 6 May 2010 (Arason et al., 2011). Based on these data, fictitious plume height data streams from two X-band radars (ISX1 and ISX2, stationed at Gunnarsholt and Klaustur, South Iceland, located 83 km to the East and 38 km to the West of the vent of Eyjafjallajökull, respectively) were generated by adding normally distributed noise with a standard deviation of 0.3 km.

The real and fictitious streamed data from all three sensors, ISKEF, ISX1 and ISX2 can be found in supplement S3, under "scenario_II" and the plots produced by FOXI.py for this simulation are presented in Fig. 12–14.

In this scenario, the plume top remained at a similar level throughout the whole period, with an exception at around 960 min after the start of simulation, when it reaches a maximum height of approx. 5.0 km above the vent (see Fig. 12a). No wind distortion in East-West direction was simulated (Fig. 12b), and the number of data streamed was constantly on a relatively high level of at least 8 data points per run, i.e. each time REFIR computed the MER with a reiteration rate of 5 min. In a real scenario such an abundance of data points, together with the fact that the plume heights did not significantly differ by sources (Fig. 12b), would provide confidence that the plume height and MER estimations by REFIR are based on consistent data from reliable data streams. We note that in this scenario we assumed the differences between the signal of ISKEF and those of ISX1, ISX2 to be relatively small, in order to have enough data for demonstration. Since the X-band sensors are mobile and have a higher vertical resolution than the C-band radar, the deviations of the first from the latter might be significantly larger in real events. This would become apparent in the source-specific plume height plots (such as Fig. 12). In such a case, with ISKEF being significant higher or lower than ISX1 and ISX2, it would be advisable to rely only on the sensors with higher resolution and switch off the C-Band radar channel.

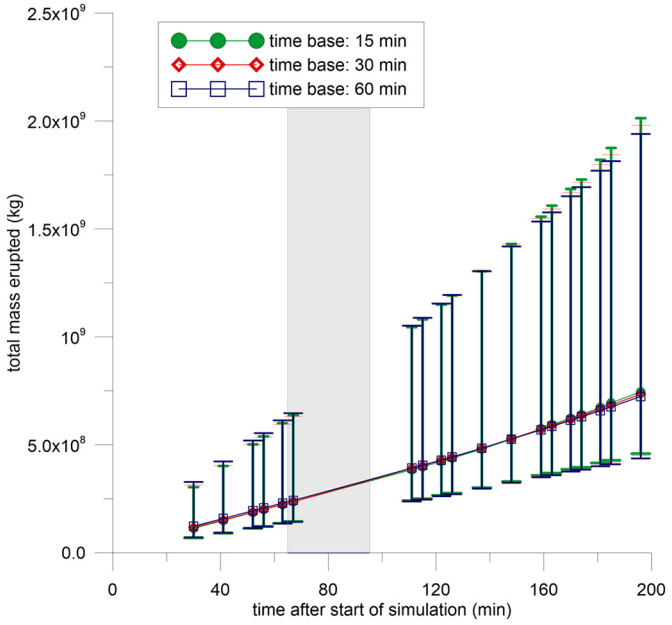

Fig. 16. Scenario III – Eyjafjallajökull, 2010: Total mass erupted as a function of time computed for the simulations of scenarios IIIa-c. The data set on which this situation was based featured a data gap between minute 65 and 95 (grey box). Error bars indicate the corresponding values for $CMER_{lower}$ and $CMER_{upper}$.

The plume height values above sea level used (after been converted to heights above vent h) as input for the REFIR internal models are displayed in Fig. 13b. It is not surprising that the resulting MER predictions for the individual models show a peak coinciding with the moment when the plume heights reach their peak (see Fig. 14a).

At this point the final best value for MER was estimated by FOXI.py to have ranged between 0.9×10^5 kg/s ($FMER_{min}$) and 2.9×10^5 kg/s ($FMER_{max}$) (Fig. 14b) and the curve for the overall mass erupted as a function of time shows a clear kink (Fig. 13c). According to the REFIR results, the total mass erupted on 6 May 2010 was between 1.7×10^9 kg and 8.0×10^9 kg.

Again, these results are based on a fictitious scenario, in which X-band radar stations provided radar data. When using exclusively the actually recorded data by the radar station ISKEF, REFIR provides *FMER* values ranging between 3.5×10^4 kg/s and 1.7×10^5 kg/s.

Table 6
Effect of data gap of 40 min duration on the amount of data sets *N* stored within the REFIR-internal data stack, demonstrated for scenario IIIa. The first row shows the time since eruption start (see also Fig. 15a–c). Rows 2–4 (marked in green) provides the number of data sets within the according bin, with Δt being the "age" of the data since recording. Every 5 min, with each reiteration of REFIR, the data sets are passed to the next bin (i.e., next row). According to the time base settings, all data sets older than 15 min are discarded (number of data sets discarded are marked in red). Thus *N*, which is presented in the bottom row (blue) gives the sum of the values in the first three bins. With the incoming data stream ceasing, *N* stepwise decreases to 0. This development is also reflected in the N-plot, shown in Fig. 15a.

Time after eruption start (min)	60	65	70	75	80	85	90	95	100	105	110	115	120
New data ($\Delta t < 5$ min)	3	data gap								3	3	3	3
5 min < Δt < 10 min	3	3	0	0	0	0	0	0	0	0	3	3	3
10 min < Δt < 15 min	3	3	3	0	0	0	0	0	0	0	0	3	3
Discarded (Δt > 15 minutes)	3	3	3	3	0	0	0	0	0	0	0	0	3
N	**9**	**6**	**3**	**0**	**0**	**0**	**0**	**0**	**0**	**3**	**6**	**9**	**9**

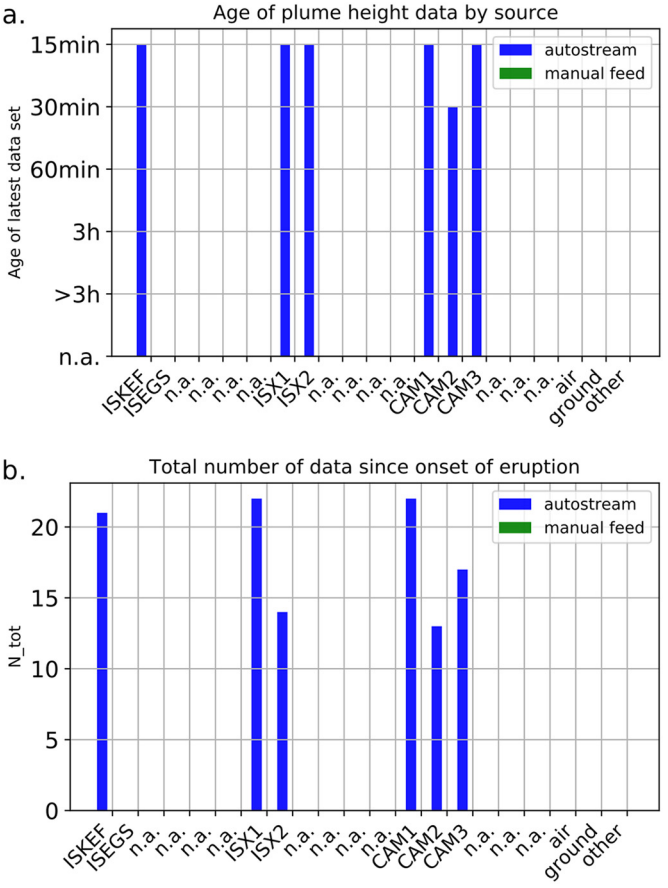

Fig. 17. Plots provided by REFIR in the activated "analysis" mode. This mode should assist the user in monitoring the situation on incoming data. The plots present, separated by data channel, the age of the latest received datum (a) and the total number of data provided (b.), separated by data channel.

These estimates are in good agreement with estimates based on real-time deposit sampling, suggesting the MER ranged between 6.2 $\times 10^4$ and $1.0 \pm 0.2 \times 10^5$ kg/s on this day (Bonadonna et al., 2011).

4.3. Simulated scenario III: simulation of a data set with a 40 min data gap, based on Eyjafjallajökull 2010 eruption (6 May 2010)

In this scenario we demonstrate the effect of gaps in data and the selection of the time base on the computation of MER in REFIR. For this purpose, the data set used in scenario II was cropped, resulting in a data subset of 3 h duration, based on the plume heights recorded on 6 May, 12:00–15:00UTC. Subsequently, within this data set, all plume height records between 13:01 and 13:41 were blanked out, simulating a complete lack of plume height information in this period (61–101 min after onset, see also Table 4). Scenario III was simulated with three different time base settings: 15 min (IIIa), 30 min (IIIb) and 60 min (IIIc).

The results are presented in Fig. 15 and in Table 5. In scenario IIIa and IIIb, the data gap is clearly reflected in the N-plots. Table 6 demonstrates for scenario IIIa how the 40 min long gap of incoming data affects *N* for each run of REFIR. According to the time base setting of this scenario, the stop in the streaming of incoming data will cause REFIR running out of information after a temporal delay of 15 min (see also Fig. 15a). As described above, FOXI.py then skips the computation of MER for the respective runs and pauses. At the moment new data are available, FOXI.py computes the newest plume height, MER and erupted mass values and linearly interpolates the missing values in between, using the last estimate computed before the gap as starting point. In scenario IIIc, however, the selected time base is large enough to ensure FOXI.py updates the estimates quasi continuously (with five minute steps) without pausing.

As reflected in Fig. 16 and Table 5, the interpolated estimates of the three scenarios tested (IIIa–c) show a relatively low deviation, compared to the range of computed uncertainty. However, in this test case the plume heights did not change considerably within the time gap simulated. It can be expected that the deviations increase significantly when facing a larger data gap in combination with distinct changes in plume heights. It is important to adjust the time base according to the update frequency of the plume height data but also to the transient characteristics of the ash column itself. For example, during a slowly changing long-lived eruption, the 3 h window may work well, but for shorter and fast changing events the results may be inaccurate.

Therefore, it is recommended to monitor the N-plots while running REFIR and finding the optimal time base. It should be large enough to avoid a data gaps and small enough to resolve any changes in plume heights on a short time scale.

5. Recommended strategies for using REFIR to obtain optimal estimates on plume heights and MER

5.1. Selecting settings for optimal plume height estimates

One of the two eruption source parameters provided by REFIR is the constrained plume height. During eruptions, the plume height sensors overview and control panel should be continuously monitored (see Fig. 3b) as well as the source- and sector-specific plume height plots (see Fig. 8 and Fig. 9a). The overview and control panel reveals if new data streams are available online. The plume height plots assist the user to identify outliers, which might indicate that the recording sensor is providing plume height data of lower quality.

As a general guidance, it is recommended to switch the data channel of low-quality plume height sensors off, since including them will not improve the final estimate of plume height, as long as data of higher quality are available.

Table 7
Suggestion for model weight factor settings. Upper row gives ratio of model weight factors of the REFIR internal 0D models in the order: w_1: w_2: w_3: w_4: w_5. Ratio in brackets provides suggestion for the weight factors [w_{1-5}: w_6] for monitoring eruptions of one of the nine volcanoes listed in the default FutureVolc configuration.

Plume	Information available	Eruption magnitude		
		Weak	Medium	Strong
Vertical	Few	4:2:2:1:1 [5:1]	4:2:2:1:1 [5:1]	2:4:4:0:1 [5:1]
	Sufficient[a]	1:1:1:1:6 [1:5]	1:1:1:1:6 [1:5]	1:1:1:1:6 [1:5]
Bent-over	Few	0:1:1:4:1 [5:1]	1:1:1:6:1 [5:1]	1:2:2:1:1 [5:1]
	Sufficient[a]	0:0:0:1:6 [1:5]	0:1:1:3:6 [1:5]	0:1:1:1:6 [1:5]

[a] Sufficient data available on magmatic temperature and atmospheric parameters.

However, in case of volcanic plumes characterized by rapidly-changing height and few measurements of high-quality available, it could still be useful to include low quality data, since the error made by using a poor quality data set with large uncertainty might still be smaller than the one resulting from the interpolation of few accurate measurements over a large time interval.

In order to support the decision-making, REFIR offers the option to activate an "analysis mode", which provides additional plots showing - separated by data channel- both the age of the latest received data (Fig. 17a) and the total number of data received since REFIR was started (Fig. 17b).

For example, Fig. 17a would indicate that the current plume height is estimated on the basis of six automatic data-streams, from which five provided data within the last 15 min. Plume height data from sensor CAM2, however, are between 30 and 15 min old. Hence, if a time base of 15 min has been selected. REFIR would not consider data coming from this source. The longest bars in Fig. 17b suggest that most data has originated from the sensors CAM1 and ISX1, closely followed by ISKEF. Since within a selected time base each plume height datum is weighed equally, this plot could indicate, that data from these three sensors have the biggest impact on estimates provided by REFIR and are hence of particular importance.

5.2. Defining the optimal time base

The choice of the best time base is a compromise between the need to get an accurate evaluation of h and to consider the most up-to-date plume height observations. For an eruption lasting longer than the longest time base allowed by REFIR (i.e., 3 h), the choice of a long time base would allow more plume height data to be processed, hence significantly reducing the uncertainty. However, if that long-lasting eruption is characterized by a plume with a continuously changing maximum height, the best estimate of plume height would be affected by outdated older data. In such a case, a shorter time base is recommended, provided it guarantees a reasonable number of data points. The choice of the time base is therefore driven by the user's expertise, knowledge of the volcano under observation and the type and evolution of the ongoing eruption. As a rule of thumb, a long time base may be the best choice for a sustained stable eruptive plume, while a short time base is better for a temporally varying weak plume.

5.3. Selecting suitable model weight factors to optimize results

The MER estimation depends significantly on the way the models are weighted, using the model-specific weight factors w_i, (e.g., see Eq. (13)), w_{1-5} and w_6 (e.g., see Eq. (16)).

The user's decision should be based on four factors: the location of the eruption site, the availability of reliable information, the magnitude of eruption and the meteorological situation. Table 7 provides an example for how these settings could be assigned.

If an eruption of one of the nine volcanoes listed within the default "FutureVolc setup" is monitored (see Fig. 1), high weight may be put on the external 1D **PlumeRise** model - provided that the information on crucial parameters (e.g., on wind speed and magmatic temperature) are considered to be reliable. For eruptions at locations other than the pre-defined volcanos within the default "FutureVolc setup" (e.g., Snæfellsjökull), the current version of REFIR does not allow application of **PlumeRise** ($w_6 = 0$).

As demonstrated in Table 7, depending on the availability and reliability of information on magmatic and atmospheric parameters, the user can decide whether to assign more weight to the simple 0D models (w_1, w_2, w_3), or to the more complex wind-affected 0D model (w_5).

A strategy might be to start with high weight on the simple models at the beginning of the eruption, until more information (e.g. on the magmatic composition and hence on the magmatic temperature) becomes available. The **Gudmundsson** model (w_4) can be useful if independent information on the MER (e.g. by real-time deposit measurements, Bonadonna et al. 2016) has been assessed and a value for the scaling parameter k_l can be estimated (see Eq. (10)). This model might provide good estimates for wind-affected medium magnitude eruptions comparable to the phases of Eyjafjallajökull 2010, hence we suggest to increase w_4 for bent-over plumes of eruptions with weak or medium magnitude (see Table 7).

In a situation when meteorological conditions or direct observations of the plume suggest that wind effects are significant (lower half of Table 7), the weighting given to the wind-blown model (w_5) can be increased. However, also the empirical models are calibrated on a dataset that includes eruption columns rising in a windy atmosphere (see Woodhouse et al. 2013; Aubry et al. 2017), so these relationships remain informative in this situation and we expect that the corresponding model weights (w_2, w_3) would be non-zero, but it may be appropriate to give very little or no weighting to the theoretical **Wilson Walker** model (w_1) derived for a plume rising in a quiescent atmosphere.

5.4. Settings for best synergy effects with external systems

Before external data - either from the experimental sensors introduced in Section 3.2.2 or obtained from other sources (e.g., from satellites) -, can be effectively used in combination with REFIR, it is crucial to know which weight factors f_i, in Eq. (19) and a_i, in Eq. (20), as well as which ratio for a_{conv}: a_{exp}: a_{man} have to be selected for best accuracy.

As a tuning strategy we recommend to use data sets on eruptions already monitored with these systems for inter-comparison studies by re-running these scenarios repeatedly to find out the optimal REFIR settings as well as the conditions under which the new components can be trusted (and hence weighed) most.

By using REFIR both for simulating past scenarios with known eruption source parameters and for monitoring ongoing eruptions, possibly in contexts other than Iceland, it is expected that a wider knowledge on the best configuration parameters (namely, weight factors) will be acquired. This would let REFIR be more "autonomous" and less dependent on the particular scenario, which is a fundamental step towards the development of an operational tool that can be used globally.

6. Conclusions and outlook

In this article we have presented REFIR, a new tool for estimating the Mass Eruption Rate (MER) of explosive volcanic eruptions in near real-time. Following a structured approach to combine disparate data streams of plume observation and accounting for the different level of accuracy of the individual measurements, the system provides a constrained estimate of the current plume height and its range of accuracy. These data are further processed by combining methods for estimating the MER using a suite of plume models. In addition, REFIR offers the possibility to consolidate data from emerging technologies and research tools. The results are then statistically combined, and a near real-time "best estimate of MER" ("FMER") is obtained together with the related level of uncertainty. Since this parameter can be used as an input for ash dispersion modelling applications, the application of REFIR at volcano observatories can contribute to early warning and an enhanced prediction of ash concentrations in the atmosphere.

The presented version of REFIR is ready for operational use. It provides, however, space for future upgrades, which, among all possible improvements and future refinement, could consist of:

- the option to retrieve relevant atmospheric data via automated data streams. This is already implemented in the PlumeRise/FOXI interface for data streamed from IMO radiosonde soundings, but can be enhanced by implementing it in a future version of FOXI.py itself.
- the possibility to explore complementary approaches to automatically discriminate between vertical and bent-over plumes, for example by

computing dimensionless wind speeds and referring to historic eruptions (Mastin, 2014).

- the option to include and process remote sensing (e.g. satellite) data and/or plume height estimates retrieved from them, such as systems developed for volcanic cloud dispersion modelling during volcanic crises.
- the implementation of additional models into FOXI.py, in order to complement the current 0D models for enhanced CMER estimates. This addition can comprise both 0D models, such as the relationship presented in Woodhouse et al. (2013), and 1D models. That would allow, for example, to run PlumeRise directly within FOXI.py, avoiding the external route, which is FutureVolc-specific and hence currently not directly applicable to other volcanic settings. Furthermore, the implementation of an additional time-dependent 1D models (such as e.g., Woodhouse et al., 2016) is planned in order to increase the capability of REFIR to monitor also unsteady, "pulsed" eruptions, as it was observed in Eyjafjallajökull 2010 (Dürig et al., 2015b).
- the option to develop a decision tree that will provide guidance to the operator on recommended weight factors for different styles of eruptions and atmospheric conditions. This is of special interest as more experience is gained in recurring eruptions, both regarding simulations and field observations. In the long term, such a decision tree might form the basis for a fully autonomous version of REFIR, which automatically adjusts the weight factors to provide estimates with optimal precision.

Acknowledgements

The development of REFIR has been part of the FUTUREVOLC supersite project and was funded by the European Union's Seventh Programme for research, technological development and demonstration under grant agreement No 308377. TD's work was also funded by the project EVER-EST, as part of the EU's Horizon 2020 research and innovation programme under grant agreement no 674907. FD publishes with permission of the Executive Director of the British Geological Survey (UKRI). Costanza Bonadonna is gratefully acknowledged for reading and commenting an earlier version of the manuscript. Susan C. Loughlin, Thordur Arason, Frank Marzano, Frances Beckett, Maurizio Ripepe, Bernd Zimanowski, Arve Kylling, Bo Galle, Fred J. Prata, Helen Thomas, Alessandro Aiuppa, Jeremy Philips, Freysteinn Sigmundsson and all the other FutureVolc collaborators are thanked for very fruitful discussions, which influenced and supported the development of REFIR. Special thanks go to Caro Ader for her help to get REFIR a lot more user friendly. We thank Larry Mastin and Lucia Gurioli whose constructive suggestions helped to improve and clarify this manuscript. Thordís Högnadóttir is gratefully acknowledged for providing the map shown in Fig. 1.

References

Arason, Th., Peterson, G.N., Bjornsson, H., 2011. Observations of the altitude of the volcanic plume during the eruption of Eyjafjallajökull, April–May 2010. Earth Syst. Sci. Data 3:9–17. https://doi.org/10.5194/essd-3-9-2011.

Aubry, T.J., Jellinek, A.M., Carazzo, G., Gallo, R., Hatcher, K., Dunning, J., 2017. A new analytical scaling for turbulent wind-bent plumes: comparison of scaling laws with analog experiments and a new database of eruptive conditions for predicting the height of volcanic plumes. J. Volcanol. Geotherm. Res. 343. https://doi.org/10.1016/j.jvolgeores.2017.07.006.

Barsotti, S., Neri, A., Scire, J.S., 2008. The VOL-CALPUFF model for atmospheric ash dispersal: 1. Approach and physical formulation. J. Geophys. Res. Solid Earth 113:B3. https://doi.org/10.1016/j.jvolgeores.2009.01.008.

Baxter, P.J., Bonadonna, C., Dupree, R., Hards, V.L., Kohn, S.C., Murphy, M.D., Nichols, A., Nicholson, R.A., Norton, G., Searl, A., Sparks, R.S.J., Vickers, B.P., 1999. Cristobalite in volcanic ash of the Soufriere Hills Volcano, Montserrat, British West Indies. Science 283, 1142–1145.

Bjornsson, H., Magnusson, S., Arason, Th., Petersen, G.N., 2013. Velocities in the plume of the 2010 Eyjafjallajökull eruption. J. Geophys. Res. Atmos. 118:1–14. https://doi.org/10.1002/jgrd.50876.

Blong, R.J., 1981. Some effects of tephra falls on buildings. In: Self, S., Sparks, R.S.J. (Eds.), Tephra Studies. NATO Advanced Study Institutes Series (Series C — Mathematical and Physical Sciences) 75. Springer, Dordrecht:pp. 405–420. https://doi.org/10.1007/978-94-009-8537-7_27.

Bonadonna, C., Genco, R., Gouhier, M., Pistolesi, M., Cioni, R., Alfano, F., Hoskuldsson, A., Ripepe, M., 2011. Tephra sedimentation during the 2010 Eyjafjallajökull eruption (Iceland) from deposit, radar, and satellite observations. J. Geophys. Res. Solid Earth 116:B12202. https://doi.org/10.1029/2011JB008462.

Bonadonna, C., Folch, A., Loughlin, S., Puempl, H., 2012. Future developments in modelling and monitoring of volcanic ash clouds: outcomes from the first IAVCEI-WMO workshop on ash dispersal forecast and civil aviation. Bull. Volcanol. 74:1–10. https://doi.org/10.1007/s00445-011-0508-6.

Bonadonna, C., Pistolesi, M., Cioni, R., Degruyter, W., Elissondo, M., Baumann, V., 2015. Dynamics of wind-affected volcanic plumes: the example of the 2011 Cordón Caulle eruption, Chile. J. Geophys. Res. Solid Earth 120 (4):2242–2261. https://doi.org/10.1002/2014JB011478.

Bonadonna, C., Delle Donne, D., Höskuldsson, Á., Marchetti, Pioli, L., Pistolesi, M., 2016. Grain-size distribution analysis from the tephra fallout instrument system in real-time. Futurevolc Rep. D7, 5.

Bursik, M., 2001. Effect of wind on the rise height of volcanic plumes. Geophys. Res. Lett. 28:3621–3624. https://doi.org/10.1029/2001GL013393.

Büttner, R., Zimanowski, B., Röder, H., 2000. Short-time electrical effects during volcanic eruption: experiments and field measurements. J. Geophys. Res. 105:2819–2827. https://doi.org/10.1029/1999JB900370.

Calvari, S., Büttner, R., Cristaldi, A., Dellino, P., Giudicepietro, F., Orazi, M., Peluso, R., Spampinato, L., Zimanowski, B., Boschi, E., 2012. The 7 September 2008 Vulcanian explosion at Stromboli volcano: multiparametric characterization of the event and quantification of the ejecta. J. Geophys. Res. 117:B5. https://doi.org/10.1029/2011JB009048.

Carazzo, G., Kaminski, E., Tait, S., 2008. On the rise of turbulent plumes: quantitative effects of variable entrainment for submarine hydrothermal vents, terrestrial and extra terrestrial explosive volcanism. J. Geophys. Res. 113:B9. https://doi.org/10.1017/S002211200500683X.

Cerminara, M., Esposti Ongaro, T., Valade, S., Harris, A.J., 2015. Volcanic plume vent conditions retrieved from infrared images: a forward and inverse modeling approach. J. Volcanol. Geotherm. Res. 300:129–147. https://doi.org/10.1016/j.jvolgeores.2014.12.015.

Cerminara, M., Esposti Ongaro, T., Berselli, L.C., 2016a. ASHEE-1.0: a compressible, equilibrium–Eulerian model for volcanic ash plumes. Geosci. Model Dev. 9:697–730. https://doi.org/10.5194/gmd-9-697-2016.

Cerminara, M., Esposti Ongaro, T., Neri, A., 2016b. Large eddy simulation of gas–particle kinematic decoupling and turbulent entrainment in volcanic plumes. J. Volcanol. Geotherm. Res. 326:143–171. https://doi.org/10.1016/j.jvolgeores.2016.06.018.

Chen, W.R., Zhao, L.R., 2015. Volcanic ash and its influence on aircraft engine components. Process. Eng. 99:795–803. https://doi.org/10.1016/j.proeng.2014.12.604.

Costa, A., Macedonio, G., Folch, A., 2006. A three-dimensional Eulerian model for transport and deposition of volcanic ashes. Earth Planet. Sci. Lett. 241:634–647. https://doi.org/10.1016/j.epsl.2005.11.019.

Costa, A., Suzuki, Y.J., Cerminara, M., Devenish, B.J., Ongaro, T.E., Herzog, M., Van Eaton, A.R., Denby, L.C., Bursik, M., Vitturi, M.D.M., Engwell, S., 2016. Results of the eruptive column model inter-comparison study. J. Volcanol. Geotherm. Res. 326:2–25. https://doi.org/10.1016/j.jvolgeores.2016.01.017.

Damby, D.E., Horwell, C.J., Larsen, G., Thordarson, Th., Tomatis, M., Fubini, B., Donaldson, K., 2017. Assessment of the potential respiratory hazard of volcanic ash from future Icelandic eruptions: a study of archived basaltic to rhyolitic ash samples. Environ. Health 16:1 -Glob. https://doi.org/10.1186/s12940-017-0302-9.

Degruyter, W., Bonadonna, C., 2012. Improving on mass flow rate estimates of volcanic eruptions. Geophys. Res. Lett. 39, L16308. https://doi.org/10.1029/2012GL052566.

Degruyter, W., Bonadonna, C., 2013. Impact of wind on the condition for column collapse of volcanic plumes. Earth Planet. Sci. Lett. 377-378:218–226. https://doi.org/10.1016/j.epsl.2013.06.041.

Dellino, P., Gudmundsson, M.T., Larsen, G., Mele, D., Stevenson, J.A., Thordarson, T., Zimanowski, B., 2012. Ash from the Eyjafjallajökull eruption (Iceland): fragmentation processes and aerodynamic behavior. J. Geophys. Res. 117:B9. https://doi.org/10.1029/2009JB006781.

Dellino, P., Dioguardi, F., Mele, D., D'Addabbo, M., Zimanowski, B., Büttner, R., Doronzo, D.M., Sonder, I., Sulpizio, R., Dürig, T., La Volpe, L., 2014. Volcanic jets, plumes and collapsing fountains: evidence from large-scale experiments, with particular emphasis on the entrainment rate. Bull. Volcanol. 76:834. https://doi.org/10.1007/s00445-014-0834-6.

Devenish, B.J., 2013. Using simple plume models to refine the source mass flux of volcanic eruptions according to atmospheric conditions. J. Volcanol. Geotherm. Res. 256:118–127. https://doi.org/10.1016/j.jvolgeores.2013.02.015.

Dioguardi, F., Dürig, T., Engwell, S.L., Gudmundsson, M.T., Loughlin, S.C., 2016. Investigating source conditions and controlling parameters of explosive eruptions: some experimental-observational- modelling case studies. In: Nemeth, K. (Ed.), Updates in Volcanology - From Volcano Modelling to Volcano Geology. InTech, Zagreb https://doi.org/10.5772/63422.

Donnadieu, F., Freville, P., Hervier, C., Coltelli, M., Prestifilippo, Valade, S., Rivet, S., Caucault, P., 2016. Near-source Doppler radar monitoring of tephra plumes at Etna. J. Volcanol. Geotherm. Res. 312:26–39. https://doi.org/10.1016/j.jvolgeores.2016.01.009.

Durant, A.J., Bonadonna, C., Horwell, C.J., 2010. Atmospheric and environmental impacts of volcanic particulates. Elements 6:235–240. https://doi.org/10.2113/gselements.6.4.235.

Dürig, T., Gudmundsson, M.T., Dellino, P., 2015a. Reconstruction of the geometry of volcanic vents by trajectory tracking of fast ejecta - the case of the Eyjafjallajökull 2010 eruption (Iceland). Earth Planets Space 67:1636. https://doi.org/10.1186/s40623-015-0243-x.

Dürig, T., Gudmundsson, M.T., Karmann, S., Zimanowski, B., Dellino, P., Rietze, M., Büttner, R., 2015b. Mass eruption rates in pulsating eruptions estimated from video analysis of the gas thrust–buoyancy transition – a case study of the 2010 eruption of Eyjafjallajökull, Iceland. Earth Planets Space 67:180. https://doi.org/10.1186/s40623-015-0351-7.

Esposti Ongaro, T., Cavazzoni, C., Erbacci, G., Neri, A., Salvetti, M.V., 2007. A parallel multiphase flow code for the 3D simulation of explosive volcanic eruptions. Parallel Comput. 33:541–560. https://doi.org/10.1016/j.parco.2007.04.003.

Folch, A., 2012. A review of tephra transport and dispersal models: evolution, current status, and future perspectives. J. Volcanol. Geotherm. Res. 235-236:96–115. https://doi.org/10.1016/j.jvolgeores.2012.05.020.

Folch, A., Costa, A., Macedonio, G., 2009. FALL3D: a computational model for transport and deposition of volcanic ash. Comput. Geosci. 35 (6):1334–1342. https://doi.org/10.1016/j.cageo.2008.08.008.

Giehl, C., Brooker, R.A., Marxer, H., Nowak, M., 2017. An experimental simulation of volcanic ash deposition in gas turbines and implications for jet engine safety. Chem. Geol. 461:160–170. https://doi.org/10.1016/j.chemgeo.2016.11.024.

Gouhier, M., Harris, A.J.L., Calvari, S., Labazuy, P., Guéhenneux, Y., Donnadieu, F., Valade, S., 2012. Lava discharge during Etna's January 2011 fire fountain tracked using MSG-SEVIRI. Bull. Volcanol. 74:787–793. https://doi.org/10.1007/s00445-011-0572-y.

Gouhier, M., Guillin, A., Azzaoui, N., Eychenne, J., Valade, S., 2015. Source mass eruption rate retrieved from satellite-based data using statistical modelling. Geophys. Res. Abstr. 17, EGU2015-10222-1.

Gudmundsson, M.T., Thordarson, T., Höskuldsson, Á., Larsen, G., Björnsson, H., Prata, F.J., Oddsson, B., Magnusson, E., Högnadottir, T., Petersen, G.N., Hayward, C.L., Stevenson, J.A., Jonsdottir, I., 2012. Ash generation and distribution from the April–May 2010 eruption of Eyjafjallajökull, Iceland. Sci. Rep. 2:572. https://doi.org/10.1038/srep00572.

Gudmundsson, M.T., Högnadóttir, T., Dürig, T., Höskuldsson, Á., Björnsson, H., Oddsson, B., Ágústsdóttir, T., 2015. Field laboratory, aircraft observations and radars. Futurevolc Rep. D7, 2.

Guffanti, M., Tupper, A., 2015. Volcanic ash hazards and aviation risk. In: Shroder, J.F., Papale, P. (Eds.), Volcanic Hazards, Risks and Disasters. Elsevier, Boston:pp. 87–108 https://doi.org/10.1016/B978-0-12-396453-3.00004-6.

Guffanti, M., Casadevall, T.J., Budding, K.E., 2010. Encounters of Aircraft with Volcanic Ash Clouds: A Compilation of Known Incidents, 1953–2009. US Dep. Int., US Geol. Surv, Reston (VA).

Haraldsson, K., 2001. Heklugosid 2000—Dreifing gjosku fra fyrsta gosdegi a landi. (in Icelandic: The Hekla 2000 eruption—distribution of ash from the first days of the eruption). BS Thesis. University of Iceland (34 pp).

Harris, A.J.L., Gurioli, L., Hughes, E.E., Lagreulet, S., 2012. Impact of the Eyjafjallajökull ash cloud: a newspaper perspective. J. Geophys. Res. 117:B9. https://doi.org/10.1029/2011JB008735.

Hewett, T.A., Fay, J.A., Hoult, D.P., 1971. Laboratory experiments of smokestack plumes in a stable atmosphere. Atmos. Environ. 5:767–789. https://doi.org/10.1016/0004-6981(71)90028-X.

Horwell, C.J., Baxter, P.J., 2006. The respiratory health hazards of volcanic ash: a review for volcanic risk mitigation. Bull. Volcanol. 69, 1–24.

Höskuldsson, A., Oskarsson, N., Pedersen, R., Grönvold, K., Vogfjörð, K., Ólafsdóttir, R., 2007. The millennium eruption of Hekla in February 2000. Bull. Volcanol. 70:169–182. https://doi.org/10.1007/s00445-007-0128-3.

Jenkins, S.F., Wilson, T., Magill, C., Miller, V., Stewart, C., Blong, R., Marzocchi, W., Boulton, M., Bonadonna, C., Costa, A., 2015. Volcanic ash fall hazard and risk. In: Loughlin, S.C., Sparks, S., Brown, S.K., Jenkins, S.F., Vye-Brown, C. (Eds.), Global Hazards and Risk. Cambridge University Press, United Kingdom. ISBN: 978-1-107-11175-2.

Johnson, J.B., Ripepe, M., 2011. Volcano infrasound: a review. J. Volcanol. Geotherm. Res. 206:61–69. https://doi.org/10.1016/j.jvolgeores.2011.06.006.

Jones, A., Thomson, D., Hort, M., Devenish, B., 2007. The U.K. Met Office's Next-Generation Atmospheric Dispersion Model, NAME III. In: Borrego, C., Norman, A.L. (Eds.), Air Pollution Modeling and Its Application XVII. Springer, USA https://doi.org/10.1007/978-0-387-68854-1_62.

Lacasse, C., Karlsdóttir, S., Larsen, G., Soosalu, H., Rose, W.I., Ernst, G.G.J., 2004. Weather radar observations of the Hekla 2000 eruption cloud, Iceland. Bull. Volcanol. 66:457–473. https://doi.org/10.1007/s00445-003-0329-3.

Macedonio, G., Costa, A., Folch, A., 2016. Uncertainties in volcanic plume modeling: a parametric study using FPLUME. J. Volcanol. Geotherm. Res. 326:92–102. https://doi.org/10.1016/j.jvolgeores.2016.03.016.

Marzano, F.S., Picciotti, E., Di Fabio, S., Montopoli, M., Mereu, L., Degruyter, W., Bonadonna, C., Ripepe, M., 2016. Near-real-time detection of tephra eruption onset and mass flow rate using microwave weather radar and infrasonic arrays. IEEE Trans. Geosci. Remote Sens. 54 (11), 6292–6306.

Mastin, L.G., 2014. Testing the accuracy of a 1-D volcanic plume model in estimating mass eruption rate. J. Geophys. Res. Atmos. 119:2474–2495. https://doi.org/10.1002/2013JD020604.

Mastin, L.G., Guffanti, M., Servranckx, R., Webley, P., Barsotti, S., Dean, K., Durant, A., Ewert, J.W., Neri, A., Rose, W.I., Schneider, D., Siebert, L., Stunder, B., Swanson, G., Tupper, A., Volentik, A., Waythomas, C.F., 2009. A multidiciplinary effort to assign realistic source parameters to models of volcanic ash-cloud transport and dispersion during eruptions. J. Volcanol. Geotherm. Res. 186:10–21. https://doi.org/10.1016/j.jvolgeores.2009.01.008.

Mastin, L.G., Randall, M.J., Schwaiger, H.F., Denlinger, R.P., 2013. Users guide and reference to ash3da three-dimensional model for eulerian atmospheric tephra transport and deposition. U.S. Geol. Surv. Open File Rep. 2013–1122 48p. http://pubs.usgs.gov/of/2013/1122/.

Morton, B.R., Taylor, G., Turner, J.S., 1956. Turbulent gravitational convection from maintained and instantaneous sources. Proc. R. Soc. Lond. A Math. Phys. Sci. 234:1–23 (1956). https://doi.org/10.1098/rspa.1956.0011.

Oberhuber, J.M., Herzog, M., Graf, H.-F., Schwanke, K., 1998. Volcanic plume simulation on large scales. J. Volcanol. Geotherm. Res. 87:29–53. https://doi.org/10.1016/S0377-0273(98)00099-7.

Oddsson, B., Gudmundsson, M.T., Larsen, G., Karlsdóttir, S., 2012. Monitoring of the plume from the basaltic phreatomagmatic 2004 Grímsvötn eruption—application of weather radar and comparison with plume models. Bull. Volcanol. 74:1395–1407. https://doi.org/10.1007/s00445-012-0598-9.

Pouget, S., Bursik, M., Johnson, C.G., Hogg, A.J., Phillips, J.C., Sparks, R.S.J., 2016. Interpretation of umbrella cloud growth and morphology: implications for flow regimes of short-lived and long-lived eruptions. Bull. Volcanol. 78:1–19. https://doi.org/10.1007/s00445-015-0993-0.

Ripepe, M., Bonadonna, C., Folch, A., Delle Donne, D., Lacanna, G., Marchetti, E., Höskuldsson, Á., 2013. Ash-plume dynamics and eruption source parameters by infrasound and thermal imagery: the 2010 Eyjafjallajökull eruption. Earth Planet. Sci. Lett. 366:112–121. https://doi.org/10.1016/j.epsl.2013.02.005.

Scollo, S., Prestifilippo, M., Pecora, E., Corradini, A., Merucci, L., Spata, G., Coltelli, M., 2014. Eruption column height estimation of the 2011–2013 Etna lava fountains. Ann. Geophys. 57 (2):0214. https://doi.org/10.4401/ag-6396.

Simkin, T., Siebert, L., Blong, R., 2001. Volcano fatalities–lessons from the historical record. Science 291:255. https://doi.org/10.1126/science.291.5502.255.

Soosalu, H., Einarsson, P., Þorbjarnardóttir, B.S., 2005. Seismic activity related to the 2000 eruption of the Hekla volcano, Iceland. Bull. Volcanol. 68:21–36. https://doi.org/10.1007/s00445-005-0417-7.

Sparks, R.S.J., 1997. Volcanic Plumes. Wiley, Chichester, New York.

Spence, R.J.S., Kelman, I., Baxter, P.J., Zuccaro, G., Petrazzuoli, S., 2005. Residential building and occupant vulnerability to tephra fall. Nat. Hazards Earth Syst. Sci. 5 (4) 477–49. https://doi.org/10.5194/nhess-5-477-2005.

Suzuki, Y.J., Costa, A., Koyaguchi, T., 2016. On the relationship between eruption intensity and volcanic plume height: insights from three-dimensional numerical simulations. J. Volcanol. Geotherm. Res. 326:120–126. https://doi.org/10.1016/j.jvolgeores.2016.04.016.

Taddeucci, J., Alatorre-Ibarguengoitia, M.A., Palladino, D.M., Scarlato, P., Camaldo, C., 2015. High-speed imaging of Strombolian eruptions: gas-pyroclast dynamics in initial volcanic jets. Geophys. Res. Lett. 42:6253–6260. https://doi.org/10.1002/2015GL064874.

Valade, S., Harris, A.J.L., Cerminara, M., 2014. Plume ascent tracker: interactive Matlab software for analysis of ascending plumes in image data. Comput. Geosci. 66:132–144. https://doi.org/10.1016/j.cageo.2013.12.015.

Walter, T.R., 2011. Structural architecture of the 1980 Mount St. Helens collapse: an analysis of the Rosenquist photo sequence using digital image correlation. Geology 39 (8):767–770. https://doi.org/10.1130/G32198.1.

Wilson, L., Walker, G.P.L., 1987. Explosive volcanic eruptions—VI. Ejecta dispersal in plinian eruptions: the control of eruption conditions and atmospheric properties. Geophys. J. R. Astron. Soc. 89, 657–679.

Wilson, T.M., Stewart, C., Sword-Daniels, V., Leonard, G.S., Johnston, D.M., Cole, J.W., Wardman, J., Wilson, G., Barnard, S.T., 2012. Volcanic ash impacts on critical infrastructure. Phys. Chem. Earth 45–46:5–23. https://doi.org/10.1016/j.pce.2011.06.006.

Wilson, G., Wilson, T.M., Deligne, N.I., Cole, J.W., 2014. Volcanic hazard impacts to critical infrastructure: a review. J. Volcanol. Geotherm. Res. 286:148–182. https://doi.org/10.1016/j.jvolgeores.2014.08.030.

Witt, T., Walter, T.R., 2017. Video monitoring reveals pulsating vents and propagation path of fissure eruption during the March 2011 Pu'u'Ō'ō eruption, Kilauea volcano. J. Volcanol. Geotherm. Res. 330:43–55. https://doi.org/10.1016/j.jvolgeores.2016.11.012.

Woodhouse, M.J., Hogg, A.J., Phillips, J.C., Sparks, R.S.J., 2013. Interaction between volcanic plumes and wind during the 2010 Eyjafjallajökull eruption, Iceland. J. Geophys. Res. Solid Earth 118:92–109. https://doi.org/10.1029/2012JB009592.

Woodhouse, M.J., Hogg, A.J., Phillips, J.C., Rougier, J.C., 2015. Uncertainty analysis of a model of wind-blown volcanic plumes. Bull. Volcanol. 77:83. https://doi.org/10.1007/s00445-015-0959-2.

Woodhouse, M.J., Phillips, J.C., Hogg, A.J., 2016. Unsteady turbulent buoyant plumes. J. Fluid Mech. 794:595–638. https://doi.org/10.1017/jfm.2016.101.

Woods, A.W., 1988. The fluid dynamics and thermodynamics of eruption columns. Bull. Volcanol. 50:169–193. https://doi.org/10.1007/BF01079681.

Zorn, E., Walter, T.R., 2016. Influence of volcanic tephra on photovoltaic (PV)-modules: an experimental study with application to the 2010 Eyjafjallajökull eruption, Iceland. J. Appl. Volcanol. 5 (1):2. https://doi.org/10.1186/s13617-015-0041-y.